A Division of Labor in the Recruitment and Topological Organization of a Bacterial Morphogenic Complex

Paul D. Caccamo[1], Maxime Jacq[1,2], Michael S. VanNieuwenhze[3,4] and Yves V. Brun[1,2] *

[1]Department of Biology, Indiana University, 1001 E. 3rd St, Bloomington, IN 47405, USA

[2]Département de Microbiologie, Infectiologie et Immunologie, Université de Montréal, Pavillon Roger-Gaudry, C.P. 6128, Succursale Centreville, Montréal, Canada

[3]Department of Molecular and Cellular Biochemistry, 212 S. Hawthorne Drive, Indiana University, Bloomington, IN 47405, USA

[4]Department of Chemistry, Indiana University, 800 East Kirkwood Avenue, Bloomington, IN 47405, USA

*** Correspondence: yves.brun@umontreal.ca (Y.V. Brun)**

Abstract

Bacteria come in an array of shapes and sizes, but the mechanisms underlying diverse morphologies are poorly understood. The peptidoglycan (PG) cell wall is the primary determinant of cell shape. At the molecular level, much of the studied morphological variation results from the regulation of PG synthesis enzymes involved in cell elongation and division. These enzymes are spatially controlled by cytoskeletal scaffolding proteins, such as FtsZ, MreB, and DivIVA, that both recruit and organize the PG synthesis complex. How then do cells define alternative morphogenic processes that are distinct from cell elongation and division? To address this question, we have turned to the specific morphotype of Alphaproteobacterial prosthecae, or "stalks". Stalk synthesis is a specialized form of zonal growth, which requires PG synthesis in a spatially constrained zone to extend a thin cylindrical projection of the cell envelope devoid of DNA and ribosomes. The morphogen SpmX defines the site of stalk PG

30 synthesis, but SpmX is a PG hydrolase. How then does a non-cytoskeletal protein,
31 SpmX, define and constrain PG synthesis to form stalks? Here we report that SpmX
32 and the bactofilin BacA act in concert to regulate stalk synthesis in *Asticcacaulis*
33 *biprosthecum*. We show that SpmX acts to recruit BacA to the site of stalk synthesis.
34 BacA then serves as a stalk-specific topological organizer that organizes PG synthesis
35 activity, including its recruiter SpmX, to the base of the stalk, where stalk PG synthesis
36 occurs. In the absence of BacA, cells produce "pseudostalks" that are the result of
37 unconstrained PG synthesis correlated with the mislocalization of SpmX. Finally, we
38 show that BacA is required to inhibit PG synthesis associated with cell
39 elongation/division and to prevent DNA entry at the site of stalk synthesis defined by
40 SpmX. Therefore, the protein responsible for recruitment of a morphogenic PG
41 remodeling complex, SpmX, is distinct from the protein that topologically organizes the
42 complex, BacA.
43

44 **Introduction**

45 Bacterial cells come in a panoply of shapes and sizes, from the ubiquitous rods and
46 cocci to hyphal, star-shaped, and appendaged bacteria [1]. In addition to shapes that
47 are reproduced faithfully across generations, bacterial cells can dynamically change
48 shape in response to environmental conditions or through a programmed life cycle [1-3].
49 The shape of most bacteria is determined by the peptidoglycan (PG) cell wall, and the
50 resulting morphology is the product of complex interactions between the proteins and
51 regulatory elements that compose the PG biosynthetic machinery. Much morphological
52 variation results from the differential regulation of divisome or elongasome proteins. For
53 example, the suppression of divisome proteins allows ovococcoid bacteria to form rods
54 under certain biofilm conditions or pathogenic rod-shaped bacteria to filament during
55 infection [3-6]. Filamentous Streptomycetes form branching hyphae by localizing the
56 same elongation machinery in different places [3, 7]. How then do cells define a new
57 morphological process that is distinct from the elongasome or divisome, but still
58 operates in the context of those critical PG synthesis modes? To address this question,
59 we have turned to the specific morphotype of Alphaproteobacterial prosthecae.

60 Prosthecae, or “stalks,” are non-essential extensions of the bacterial cell body thought
61 to play a role in nutrient uptake [8, 9]. Stalk synthesis requires PG synthesis in a
62 spatially constrained zone in order to extend a thin cylindrical projection of the cell
63 envelope. The stalk is compartmentalized from the cytoplasm, as it is devoid of DNA
64 and ribosomes and excludes even small cytoplasmic proteins such as GFP [9].
65 *Asticcacaulis biprosthecum*, a gram negative Alphaproteobacterium from the
66 Caulobacteraceae family [10], produces two bilateral stalks whose synthesis depends
67 on PG synthesis at the base of the incipient stalk structures (red arrows in Figure 1A)

68 [11]. How do cells harness PG synthesis machinery to produce stalks while preventing
69 its typical function of cell elongation or division?

70 Here we report how a recently identified class of bacterial cytoskeletal protein, known as
71 "bactofilin" (BacA), plays a dual role by defining the topography of PG synthesis for the
72 synthesis of stalks and by inhibiting a default cell elongation mode at that same site in
73 *A. biprosthecum*. Bactofilins are conserved throughout the bacterial kingdom and are
74 characterized by the presence of a central conserved DUF583 (or "bactofilin") domain
75 flanked by N- and C-terminal regions of variable length and sequence (Figure 1B) [12].
76 Bactofilins are involved in cell shape determination in a number of species. For
77 example, in the helical *Helicobacter pylori* and *Leptospira biflexa*, bactofilins are
78 required for proper helical shape generation [13, 14]. In *Caulobacter crescentus*,
79 bactofilins optimize the rate of stalk synthesis at the cell pole by a yet unknown
80 mechanism [12]. A bactofilin mutant of *C. crescentus* still synthesizes stalks normally in
81 a complex medium and exhibits a 50% reduction in stalk length under phosphate
82 starvation where stalk elongation is strongly stimulated. While bactofilin recruits PbpC,
83 whose mutant leads to a similar modest reduction in stalk length, a bactofilin mutant still
84 exhibits strong PG synthesis activity similar to wild-type cells, indicating that *C.*
85 *crescentus* bactofilin is not required for stalk PG synthesis. Therefore, it is not well
86 understood how bactofilins exert an effect on morphology, but a common theme
87 appears to be association or direct interaction with PG modifying enzymes.

88 The best studied bacterial cytoskeletal proteins (MreB, FtsZ, and DivIVA) serve dual
89 roles as both recruiters and organizers of the proteins for their respective PG synthesis
90 complexes. In contrast, we show that the roles of recruiter and organizer of PG

91 synthesis have undergone a division of labor in *A. biprosthecum* stalk synthesis, where
92 a morphogen, SpmX, recruits its own organizing cytoskeletal protein, BacA. Our prior
93 work established that the recruitment of the stalk PG synthesis machinery is performed
94 by the modular morphogen SpmX: changing SpmX location is sufficient to drive stalk
95 synthesis at a new site [11], much like changing the position of FtsZ changes the
96 location of the site of cell division. However, SpmX is a PG hydrolase, not a cytoskeletal
97 protein [11, 15]. How then does a non-cytoskeletal protein, SpmX, define and constrain
98 PG synthesis to form stalks? In this work, we identify BacA as a cytoskeletal scaffolding
99 protein that provides topological specificity to stalk PG synthesis, including to the
100 recruiter SpmX itself. We apply genetics, cell biology, microscopy, chemical labeling,
101 and quantitative analysis to examine the interconnected roles of the morphogen SpmX
102 and the bactofilin BacA in *A. biprosthecum* stalk synthesis. We present evidence that
103 SpmX and BacA act in a coordinated fashion to initiate and regulate stalk synthesis.
104 SpmX acts as the recruiter of the stalk synthesis complex, including BacA. BacA then
105 serves as a stalk-specific cytoskeletal scaffolding protein that anchors the putative
106 synthesis complex, including SpmX, to the base of the stalk, and defines the width of
107 the complex. In the absence of BacA, cells produce abnormal "pseudostalks" that are
108 the result of unconstrained PG synthesis correlated with the mislocalization of SpmX.
109 Finally, we show that BacA is required to block PG synthesis involved in cell elongation
110 and division, as well as DNA, from the site of stalk synthesis defined by SpmX.
111 Therefore, the protein responsible for recruitment of a morphogenic PG remodeling
112 complex, SpmX, is different than the protein that topologically organizes the complex,
113 BacA. Such separation of the recruitment and scaffolding activities in two different

114 proteins may prove more versatile for morphogenetic events that do not simply involve

115 modulation of cell elongation or division.

116

Results

A. biprosthecum encodes a single bactofilin gene whose product self-polymerizes *in vitro*

A. biprosthecum has proven to be a better system than *C. crescentus* to identify genes required for stalk synthesis because: 1) with the exception of a *C. crescentus* MreB-mCherry sandwich fusion that acts through an unknown mechanism to block stalk synthesis [16], the *A. biprosthecum spmX* mutant is the only known stalkless mutant in any Caulobacterales species whose phenotype is not bypassed by phosphate starvation [11, 17, 18], which stimulates stalk synthesis [11, 19-21]; 2) *A. biprosthecum* stalks are located at midcell, away from the myriad of polarly localized proteins involved in *C. crescentus* development and cell cycle progression [22-25], eliminating any potentially confounding co-localization or interaction data; and 3) many of the genetic tools developed for *C. crescentus* work in *A. biprosthecum*. In *C. crescentus*, deletion of the bactofilin genes *bacA* and *bacB* (for clarity, these will be referred to as "$bacA_{Cc}$" and "$bacB_{Cc}$") leads to a slight reduction in the length of otherwise normal stalks [12, 26, 27]. Only one bactofilin homolog was found in the *A. biprosthecum* genome, which we have named "*bacA*" due to its bidirectional best hit in *C. crescentus* being $bacA_{Cc}$ (Figure 1C). The genomic arrangement of the *A. biprosthecum bacA* locus is similar to that of *C. crescentus* $bacA_{Cc}$, with a putative M23 family metallopeptidase gene (CC1872/ABI_34190) directly upstream and overlapping the $bacA_{Cc}$/*bacA* coding regions, and a putative peroxiredoxin gene (CC1871/ABI_34200) further upstream (Figure 1C). Downstream of and convergent to *bacA* lies a hypothetical gene (Figure 1C). BacA exhibits high sequence and predicted structural similarity to the *C. crescentus* bactofilins, with a central DUF583 domain composed of repeating β strands flanked by proline-rich N- and C-termini, suggesting similar biochemical properties (Figure 1D).

142 Indeed, $BacA_{Cc}$ can self-assemble *in vitro* into filaments, filament bundles, and sheets
143 [12, 28]. To test if *A. biprosthecum* BacA is a self-polymerizing protein, we
144 overexpressed and purified both $BacA_{Cc}$ and BacA in *Escherichia coli* and visualized the
145 purified proteins via transmission electron microscopy (TEM) (Figure 1E). While $BacA_{Cc}$
146 readily polymerized in various environments (salt, pH, chaotropic agent), under similar
147 conditions BacA formed proteins aggregates instead of filaments. While most conditions
148 tested did not improve BacA solubility, addition of high detergent concentration (10%
149 Triton X-100) allowed filament formation. The TEM micrographs show that both
150 bactofilin proteins, $BacA_{Cc}$ and BacA, self-polymerize *in vitro* to form protofilament
151 bundles, with BacA forming 90 nm wide filaments made of single filaments stacked
152 together through lateral-lateral interactions, similar to $BacA_{Cc}$ (Figure 1E; red arrows
153 indicate BacA protofilaments).

154 **BacA is required for stalk synthesis**

155 In *C. crescentus*, deletion of the bactofilin homologs $bacA_{Cc}$ and/or $bacB_{Cc}$ does not
156 abrogate stalk synthesis or impact stalk ultrastructure, but results in a slight reduction in
157 stalk length under stalk synthesis-stimulating, phosphate-limited conditions, and does
158 not impact the strong PG synthesis activity at the base of the stalk [12]. This suggests
159 that, in *C. crescentus*, deletion of $bacAB_{Cc}$ affects only stalk longitudinal extension and
160 to a limited extent [12]. Strikingly, ~95% of *A. biprosthecum* Δ*bacA* mutant cells were
161 completely stalkless when grown in the rich medium PYE, with a small proportion of
162 cells exhibiting bump-like protrusions at the midcell where stalks would normally be
163 found (Figure S1). Since growth in rich medium may mask latent stalk phenotypes [11,
164 21], the Δ*bacA* mutant was studied under phosphate starvation, which stimulates stalk
165 synthesis [11, 19-21].

166 In low phosphate medium, more than half (58% ± 12%) of WT cells possessed a visible
167 cell body extension, all of which were stalks (Figure 2). In the Δ*bacA* mutant, only 3% ±
168 2% of total cells produced a stalk (Figure 2). Instead of synthesizing wildtype stalks, the
169 Δ*bacA* mutant produced short, wide protrusions at the bilateral positions where stalks
170 are normally synthesized, which we have termed “pseudostalks” (Figure 2A and red
171 arrows in Figure 2B). Under phosphate starvation, the stalks produced by WT cells were
172 7.3 ± 3.7 μm long and 171 ± 13 nm in diameter at the base (Figure 2). Pseudostalks
173 were significantly shorter than stalks at 0.9 ± 0.5 μm long (~88% decrease in length
174 compared to WT), were more variable in diameter, and were often branched or
175 "frazzled" at the ends (Figure 2). Pseudostalks were significantly wider in diameter at
176 the base, 392 ± 73 nm or an ~129% increase in width compared to WT (Figure 2).

177 The presence of a low-copy plasmid encoding *bacA* expressed from its native promoter
178 restored stalk diameter a to WT levels (178 ± 20 nm vs. 171 ± 13 nm, respectively),
179 suggesting that BacA plays a key role in determining and maintaining stalk width (Figure
180 2). In addition, 28% ± 6% of complemented Δ*bacA* cells produced WT-like stalks, a 10-
181 fold increase over the mutant (Figure 2). Complemented Δ*bacA* cells produced stalks
182 2.4 ± 2.0 μm long that, while shorter than WT stalks, were significantly longer than
183 Δ*bacA* pseudostalks (Figure 2). It is unlikely that the less efficient complementation of
184 stalk number and length are due to polarity effects of the mutation since the gene
185 downstream of *bacA* is transcribed in the opposite direction (Figure 1C). Dosage effects
186 may explain why complementation is not fully achieved for these phenotypes; however,
187 we are unable to test this at this time due to a lack of BacA antibodies. Taken together,
188 these data show that BacA is required for stalk synthesis in *A. biprosthecum*.

189 **BacA localizes to the site of stalk synthesis after SpmX localization**

190 While the localization of SpmX is known, the pattern of BacA localization is not. The
191 stalk morphogen SpmX localizes to the future site of stalk synthesis in predivisional
192 cells of *Asticcacaulis*, where it marks the site of stalk synthesis, which occurs after cell
193 division and swarmer cell differentiation in the next cell cycle (Figure 1A) [11]. To
194 investigate the subcellular localization of BacA in WT cells, we fused BacA to mVenus
195 at the native locus and performed fluorescence microscopy. This fusion is functional,
196 and cells expressing BacA-mVenus produced normal stalks at a similar frequency as
197 WT cells expressing the native protein (Figure S2).

198 We first performed time-lapse fluorescence microscopy to determine the timing of BacA
199 localization during the cell cycle (Figure 3A and Movies S1 & S2). The first four panels
200 of Figure 3A (0-84 min) show the elongation of a predivisional mother cell as it produces
201 an incipient swarmer daughter cell, where BacA is already localized at bilateral positions
202 in the stalked half of the cell. In contrast to SpmX, which localizes before cell division at
203 the future sites of stalk synthesis, we were unable to detect new BacA foci in
204 predivisional cells. After cell division (the transition from 84-112 min), a BacA-mVenus
205 focus appeared at a lateral position in the incipient swarmer cell. While only one BacA-
206 mVenus focus is visible in the overlay from 112 to 140 min, a second focus is clearly
207 visible in the overlay at 168 and 196 min. This process of BacA localization after cell
208 division is repeated in later panels with a second daughter cell (196-252 min).
209 Therefore, SpmX localizes before cell division (Figure 4A), whereas BacA localizes after
210 cell division, significantly after SpmX (Figure 3C). We then sought to quantify BacA-
211 mVenus localization at the population level, rather than single cells. Overall, BacA-
212 mVenus localized to bilateral positions at the base of the stalks (Figure 3D). A

213 population-level heatmap of the subcellular localization of BacA-mVenus foci exhibited a
214 localization pattern similar to that of SpmX (Figure 4D) [11], with foci clustering in a
215 bilateral manner at the midcell (Figure 3E).

216 **SpmX is required for BacA localization**

217 Considering that 1) both SpmX and BacA are required for WT stalk synthesis; 2) that
218 both proteins localize to the site of stalk synthesis; and 3) that SpmX localizes to the site
219 of stalk synthesis prior to BacA, we hypothesized that SpmX is required for BacA
220 localization. In order to test the role of SpmX in BacA localization, we constructed a
221 strain with a *bacA-mVenus* fusion at the native locus in the Δ*spmX* background.

222 As reported above in the WT background, BacA-mVenus localized to the base of the
223 stalk (Figure 3D, top) with foci clustering in a bilateral manner at the midcell (Figure 3E,
224 top). In the Δ*spmX* mutant, BacA-mVenus was often mislocalized toward the poles
225 (Figure 3D, bottom), and the population-level heatmap of the subcellular localization of
226 BacA-mVenus foci in the Δ*spmX* mutant showed that BacA-mVenus was randomly
227 distributed throughout the cell body (Figure 3E, bottom). However, these images
228 represent only a snapshot of BacA-mVenus localization at a single time point. To further
229 investigate BacA-mVenus dynamics in WT and Δ*spmX* strains, we performed time-
230 lapse fluorescence microscopy (Figures 3A & 3B and Movies S1-S4) and used particle
231 tracking to follow movement and velocity changes for individual foci (Figures 3F & 3G).
232 In WT cells, BacA-mVenus foci were constrained bilaterally at sites of stalk synthesis
233 and remained relatively static once they appeared (Figures 3A, 3F, & 3G and Movies S1
234 & S2). Conversely, in the Δ*spmX* mutant, BacA-mVenus foci moved randomly
235 throughout the cell body and exhibited start-stop patterns of spikes and drops in velocity

236 (Figures 3B, 3F, & 3G and Movies S3 & S4). Taken together, these data show that
237 SpmX is required for BacA localization.

238 **BacA is required to constrain SpmX at the base of the stalk**

239 Cytoskeletal scaffolding proteins can be loosely defined as proteins that physically
240 organize the molecular components of a biological process or pathway [3]. Because 1)
241 SpmX acts in a modular fashion to define the site of stalk synthesis [11]; 2) SpmX is
242 required for BacA localization; and 3) BacA is required to constrain stalk diameter, we
243 hypothesized that BacA organizes PG synthesis enzymes, and perhaps SpmX, at the
244 site of stalk synthesis. To test SpmX localization in the absence of BacA, we
245 constructed strains with a *spmX-eGFP* fusion at the native locus in both WT and Δ*bacA*
246 backgrounds.

247 Consistent with previously published results [11], fluorescence microscopy showed that
248 SpmX-eGFP first appears in the incipient swarmer compartment of predivisional cells of
249 *A. biprosthecum* where it localizes bilaterally to mark the site of stalk synthesis, which
250 occurs after cell division and swarmer cell differentiation [11] (Figures 1A, 4A, 4C, & 4D
251 and Movie S5). Interestingly, SpmX localized to the future bilateral site of stalk synthesis
252 even in the absence of BacA (Figures 4B-4D and Movie S6). However, in the Δ*bacA*
253 mutant SpmX-eGFP often localized to the tips of pseudostalks rather than the base of
254 stalks as it does in WT cells (Figure 4C). When stalk synthesis was restored in the
255 Δ*bacA* mutant by the expression of BacA from a plasmid, SpmX localization to the base
256 of the stalk was restored as well (Figure 4C). This defect of SpmX localization is further
257 revealed by the localization heatmaps, where, rather than a tight localization close to
258 the cell envelope in WT, there is a diffuse localization at the midcell that radiates away

259 from the cell body in the Δ*bacA* mutant (Figure 4D). Indeed, quantification of the
260 orthogonal distance of SpmX-eGFP maxima from the medial axis of the associated cell,
261 showed a significant increase in Δ*bacA* cells compared to WT, a defect that was
262 rescued in the complementation strain (Figure 4E). It should be noted that when stalk
263 synthesis is restored by exogenous expression of BacA, SpmX localization to the base
264 of the stalk is also restored in these cells (Figure S3). While global SpmX protein levels
265 according to Western blot are similar between WT and Δ*bacA* strains (Figure S4), the
266 area of the SpmX-eGFP maxima significantly increased in the Δ*bacA* mutant compared
267 to WT, a defect that was restored in the complementation strain (Figure 4F). This
268 suggests that BacA may play a role in regulating the number of SpmX molecules that
269 comprise the stalk synthesis complex. These results indicate a scaffolding role for BacA
270 during stalk synthesis whereby BacA is required to constrain SpmX in a tight area at the
271 base of the stalk. The above results suggest that SpmX acts upstream of BacA, which
272 was confirmed by the Δ*spmX* Δ*bacA* double mutant, which phenocopied Δ*spmX* (Figure
273 4G).

274 **BacA and SpmX colocalize *in vivo* and interact in a bacterial two-hybrid system**
275 Since SpmX is required for BacA localization (Figure 3) and BacA is required to
276 constrain SpmX at the base of the stalk (Figure 4), we wondered whether this could be
277 due to a direct interaction between the two proteins. To address this, we first
278 simultaneously expressed SpmX-mCherry and BacA-mVenus fusions in *A.*
279 *biprosthecum*. Cells produced stalks, indicating that the fusions are functional when
280 expressed together. Both BacA-mVenus and SpmX-mCherry formed foci at the midcell
281 that often overlapped (Figure 5), and there was a positive correlation between the
282 localization of the two fusion proteins (Pearson's Correlation Coefficient = 0.48 ± 0.23; n

283 = 179). We note that in many cases, one of the co-localized BacA focus was much
284 weaker than the other, with some cells having only detectable co-localized BacA with
285 one of the two SpmX foci. This may be an indication that relatively few molecules of
286 BacA are required to constrain SpmX at the base of stalks or that the BacA-SpmX
287 interaction is transitory and becomes less important as the stalk synthesis matures.

288 We then asked whether SpmX and BacA interact *in vivo* using bacterial adenylate
289 cyclase two-hybrid (BACTH) assays [29]. We tested all combinations of T18 and T25
290 fusions for SpmX and BacA (Figure 6). Serving as an internal control, both SpmX and
291 BacA showed self-interactions (Figure 6), consistent with previous results showing that
292 *C. crescentus* SpmX forms oligomers [30] and confirming our results showing BacA is a
293 self-polymerizing protein (Figure 1E). Notably, we also observed SpmX-BacA
294 interactions (Figures 6C & 6D), although the only interactions we observed were when
295 BacA was fused with the T25 fragment on the N-terminus (T25-BacA). These results
296 make sense in the context of recent work showing that the N-terminal tail of *Thermus*
297 *thermophilus* bactofilin is required for membrane binding [31]. If the BacA N-terminal tail
298 is also involved in membrane binding, the fact that we only detect SpmX-BacA
299 interactions when the C-terminal tail is unencumbered by a fusion suggests that the C-
300 terminal region of BacA is involved in protein-protein interactions with SpmX.

301 **Pseudostalks are composed of PG and formed through dispersed PG synthesis**
302 *A. biprosthecum* stalks extend through the addition of newly synthesized PG at the base
303 of the stalk and are composed of PG throughout [11]. Indeed, isolated PG sacculi
304 maintain the shape of the bacterial cell, including PG-containing stalks [32]. To test if
305 pseudostalks are composed of PG, we first isolated sacculi from *A. biprosthecum* WT

306 and Δ*bacA* cells. As expected, *A. biprosthecum* WT sacculi exhibited long and thin
307 bilateral extensions of stalk PG (Figure 7A). Sacculi purified from Δ*bacA* cells showed
308 sac-like bilateral extensions of PG that mimicked the morphology of pseudostalks
309 (Figure 7A), confirming that pseudostalks are composed of PG.

310 There are several modes of PG synthesis that could result in pseudostalks. For
311 example, they could be synthesized 1) from the base like WT stalks, albeit with a wider
312 and variable area of extension; 2) via polar growth similar to vegetative growth of the
313 filamentous Streptomycetes [3], with PG remodeling occurring through polar tip
314 extension; or 3) be the result of dispersed PG synthesis throughout the pseudostalk,
315 similar to lateral elongation of some rod-shaped cells [3].

316 To test these possibilities, we employed various methods of Fluorescent D-Amino Acid
317 (FDAA) [33] labeling to visualize active PG synthesis during growth in low-phosphate
318 medium. Cells were first subjected to short labeling pulses (45 min or ~20% of doubling
319 time) of a red FDAA (TADA) (Figure 7B). If pseudostalks are synthesized from the base,
320 the FDAA should label the cell and stalk-to-cell body junction, but not the pseudostalk
321 itself. In WT cells, labeling was diffuse throughout the cell, but absent from the stalks,
322 except from the stalk-to-cell body junction where stalk PG is synthesized (Figure 7B),
323 consistent with previous results [11]. In contrast, Δ*bacA* cells showed strong labeling
324 throughout the pseudostalks, indicating that these structures are not solely synthesized
325 from the base as in WT stalks (Figure 7B). Because the labeling time was short relative
326 to the time required for pseudostalk growth, we hypothesized that pseudostalk PG
327 synthesis occurs through PG synthesis dispersed throughout the structure rather than
328 by tip PG synthesis. To obtain better spatiotemporal resolution of PG remodeling and to

329 correlate SpmX localization with PG remodeling, we performed virtual time-lapse FDAA
330 labeling, where short successive pulses of different colored FDAA probes are used for
331 spatiotemporal labeling of areas of PG synthesis. *A. biprosthecum* WT SpmX-eGFP and
332 Δ*bacA* SpmX-eGFP cells were first labeled with a blue FDAA (HADA) for 6 min followed
333 by a red FDAA (TADA) for 3 min, with the dye being washed away after each respective
334 incubation (Figure 7C). Cells were then imaged via 3D-SIM (Structured Illumination
335 Microscopy). For WT cells, the HADA and TADA signals overlapped both in the cell
336 body and at the base of the stalk, colocalized with the SpmX-eGFP focus and
337 consistent with stalk PG synthesis at the base and no PG synthesis along the stalk
338 length (Figure 7C). In contrast, the HADA and TADA signals overlapped in both the cell
339 body and the pseudostalks of Δ*bacA* cells and with SpmX-eGFP localizing to the tips of
340 the pseudostalks (Figure 7C), indicating that pseudostalks are formed via dispersed PG
341 synthesis throughout the structure.

342 **BacA inhibits the default elongation and division modes of PG synthesis as well**
343 **as DNA entry at sites of stalk synthesis**

344 While the FDAA labeling techniques used above (Figures 7B & 7C) show that new PG
345 is incorporated into the pseudostalk, it does not distinguish *per se* if PG is being
346 incorporated from the base, as in WT stalks, or if PG incorporation is distributed
347 throughout the pseudostalk. To determine the PG incorporation pattern for Δ*bacA*
348 pseudostalks, we performed pulse-chase FDAA labeling (Figure 7D). *A. biprosthecum*
349 WT and Δ*bacA* cells were first labeled with a red FDAA (TADA) for ~12-14 hours (~3-
350 3.5 cell cycles) to ensure whole-cell labeling, including stalks and pseudostalks. Cells
351 were then washed twice to remove the FDAA and time-lapse fluorescent microscopy

352 was performed. As the *A. biprosthecum* WT cells grew, FDAA signal disappeared from
353 the cell body, but was retained in the stalk (Figure 7D), with a slight clearing near the
354 base as stalk PG was synthesized from its base (Figure 7D, yellow triangles). In
355 contrast, Δ*bacA* cells lost FDAA signal throughout both the cell body and the
356 pseudostalks at a similar rate (Figure 7D), consistent with PG synthesis throughout the
357 pseudostalk. Strikingly, 49% (42/85) of Δ*bacA* cells observed were able to extend and
358 divide from the pseudostalks and produced cell-like extensions that continued to
359 elongate after cytokinesis (Figure 7E, yellow triangles), suggesting that cell growth was
360 occurring at sites usually reserved for stalk synthesis. These results suggested that
361 BacA might be required to prevent entry of chromosomal DNA that would be required
362 for continued growth of these lateral cell extensions. To determine if Δ*bacA*
363 pseudostalks contained DNA, we stained live cells with DAPI. In WT cells, DAPI
364 staining was constrained to the cell body, but in Δ*bacA* cells, pseudostalks stained
365 strongly for DNA (Figure 7F). It should be noted that we were unable to determine the
366 viability of the cell-like structures produced from the pseudostalks, but, qualitatively,
367 there is no discernable difference between the growth of WT and Δ*bacA* strains in liquid
368 culture or on plates. Taken together, these data indicate that, in addition to providing a
369 scaffold for proper stalk PG synthesis at its base, BacA inhibits not only unwanted PG
370 synthesis involved in cell elongation and division, but also the entry of DNA at sites of
371 stalk synthesis.

372

373 **Discussion**

374 Intricate biological processes underlie even the simplest of shapes. The ubiquitous rod-
375 and sphere-shaped bacteria can be generated through multiple strategies [34, 35], but
376 the final observed form is the result of finely tuned gene expression, metabolic
377 processes that regulate PG precursor and subunit levels, and the spatiotemporal
378 localization of PG-modifying enzymes. The study of shape generation and maintenance
379 has uncovered a common theme of scaffolding proteins such as MreB, FtsZ, and
380 DivIVA that recruit and organize PG synthesis to specific subcellular locations at
381 specific times. Here we present evidence that the paradigm of a cytoskeletal scaffolding
382 protein serving the dual roles of recruitment and organization in PG synthesis is not
383 always true. In *A. biprosthecum*, the roles of recruitment and organization for the stalk
384 synthesis PG remodeling complex are performed by two distinct proteins, SpmX and
385 BacA, respectively. Furthermore, BacA prevents cell elongation and division associated
386 PG synthesis from being activated at the site of stalk PG synthesis. Finally, BacA also
387 prevents the entry of DNA into stalks.

388 Previous work has shown that SpmX appears early in *Asticcacaulis* spp. cell cycle,
389 where it localizes in pre-divisional daughter cells to mark the future site of stalk
390 synthesis [11]. Here we show that BacA operates downstream of SpmX for subcellular
391 localization in the *A. biprosthecum* stalk synthesis pathway but acts upstream of SpmX
392 for the topological organization of SpmX and the PG synthesis machinery. In the
393 absence of SpmX, cells are stalkless and BacA-mVenus forms foci that move randomly
394 throughout the cell body, indicating that SpmX recruits BacA, and presumably other PG
395 remodeling enzymes that remain to be discovered, to the site of stalk synthesis (Figure
396 7A). In a Δ*bacA* Δ*spmX* double mutant, cells phenocopy the Δ*spmX* mutant and fail to

397 produce stalks or pseudostalks (Figure 4G). This supports the conclusion that BacA
398 operates downstream of SpmX

399 Interestingly, once stalk synthesis is initiated, BacA serves as a scaffolding protein that
400 constrains PG synthesis at the base of the stalk, allowing for WT stalk elongation and
401 maturation (Figure 8A). Based on current knowledge, this is the first reported
402 morphogenic PG remodeling process in which the protein responsible for recruitment of
403 the complex is different from the scaffolding protein that organizes the complex. The
404 stalkless phenotype of *spmX* and *bacA* mutants in *A. biprosthecum* is striking compared
405 to *C. crescentus*, where neither gene is required for stalk synthesis. Deletion of $bacA_{Cc}$
406 does not impact stalk synthesis in the complex PYE medium and leads to a mild
407 reduction of stalk length only under the strong stalk elongation stimulating conditions of
408 phosphate starvation [12, 16, 36]. In *A. excentricus*, which has a single sub-polar stalk,
409 *spmX* is required for sub-polar stalk synthesis, but phosphate starvation results in polar
410 stalk synthesis in the *spmX* mutant [11]. Perhaps the synthesis of non-polar stalks has
411 additional topological constraints that are more easily solved by the separation of the
412 recruitment and scaffolding processes into two different proteins as we have described
413 here, as this separation may be more adaptable for generating unique morphologies.
414 Comparative analysis of the requirements for stalk synthesis in these three species
415 provides an excellent model to determine how evolution can solve different
416 morphological constraints.

417 Many questions remain regarding prosthecae synthesis in both *A. biprosthecum*
418 specifically and the stalked Alphaproteobacteria in general. Even among closely related
419 species there are phenotypic differences, such as the number and placement of stalks,

420 as well as differences in the genes involved in stalk synthesis. Furthermore, in many
421 stalked marine species, the stalk serves a reproductive function, with a budding
422 daughter cell produced from the tip of the stalk [37-40]. How have these stalk synthesis
423 pathways evolved? Are there core genes that are shared amongst bacteria that produce
424 stalks? There are certainly differences, specifically between *C. crescentus* and
425 *A. biprosthecum* (Table S1) [11], but what other genes are involved in *A. biprosthecum*
426 stalk synthesis? ABI_34190, the gene that lies upstream and overlaps *bacA* (Figure
427 1C), is a putative M23 family metallopeptidase (Pfam 01551) whose predicted
428 endopeptidase activity would cleave PG crosslinks. Thus, ABI_34190 provides an
429 intriguing candidate for both its predicted function in PG remodeling and its genomic
430 association with *bacA*. How do bactofilins function in stalk synthesis? Presumably, the
431 ability to self-polymerize is important to bactofilin function in general but, to date, there
432 have been no studies showing that non-polymerizing mutants lead to a phenotypic
433 change. The terminal regions flanking the conserved bactofilin domain often vary
434 between species. Do the N- and C-terminal domains serve any specific purposes? Work
435 on *T. thermophilus* bactofilin showed that the N-terminal region is involved in membrane
436 binding [31]. We used high detergent levels, a high micellization condition, to get
437 purified BacA to form filaments *in vitro*. Our BACTH results suggest that the C-terminus
438 is important for BacA-SpmX interaction. It seems likely that these N- and C- terminal
439 regions play important roles in membrane and protein interactions.

440 This study has also revealed an unexpected role for a scaffold protein in inhibiting
441 default modes of PG synthesis. In the absence of BacA, cells produce what we have
442 termed "pseudostalks", which are significantly shorter and wider than stalks. In addition,

443 BacA is required to constrain SpmX at the base of the stalk (Figure 8A), as observed by
444 the mislocalization of SpmX-eGFP in the absence of BacA (Figure 8B). Pseudostalks,
445 like WT stalks, are composed of PG. However, unlike WT stalks, which are synthesized
446 from the base of the stalk (Figure 8A), pseudostalks are the result of dispersed PG
447 remodeling throughout the structure (Figure 8B). We find a parallel for this phenomenon
448 with the cytoskeletal scaffolding protein DivIVA in the Actinobacterium *Mycobacterium*
449 *smegmatis*. Normal, rod-shaped *M. smegmatis* undergo asymmetric bipolar growth, and
450 DivIVA focuses this cell envelope assembly at the poles [41]. When DivIVA is depleted,
451 PG synthesis persists, but in a disorganized manner throughout the cell, leading to
452 spherical cells [42]. Similarly, in the absence of BacA, PG synthesis persists, but in a
453 disorganized manner leading to pseudostalks.

454 Strikingly, we show that the pseudostalks that form in the absence of BacA can
455 incorporate the default cell elongation and cell division modes, forming cell body
456 extensions that contain DNA and can divide. These results suggest that the cytoskeletal
457 bactofilin BacA not only organizes and constrains PG synthesis to specific subcellular
458 locations (Figure 8A) but also inhibits PG synthesis associated with cell elongation and
459 division and DNA entry at the site of stalk synthesis defined by SpmX. The decoupling
460 of the recruitment and scaffolding roles for proteins that localize the PG synthesis
461 complex may facilitate safeguarding against establishment of cell elongation and
462 division at those morphogenetic sites. However, removal of a single layer of regulation
463 (in this case, *A. biprosthecum* BacA) can lead to unregulated growth, with *A.*
464 *biprosthecum* becoming a branching organism via pseudostalks. This follows an
465 emerging theme of bacterial morphogenesis in which morphological variation results

466 from the differential regulation of PG remodeling [3, 43, 44]. In other words, much like
467 the Actinobacteria *Streptomyces* spp., *A. biprosthecum* localizes PG synthesis at
468 specific places with different morphological results: branching hyphae and stalks,
469 respectively. Furthermore, this result suggests that at least some of the PG synthesis
470 enzymes used for stalk synthesis are the same as those used for cell elongation and
471 division, which may explain why we have yet to identify a PG synthesis enzyme used
472 specifically for stalk synthesis.

473

474 **Methods**

475 **Bacterial strains and growth conditions**

476 All freezer stocks were maintained in 10% DMSO at -80°C.

477 *A. biprosthecum* strains used in this study were grown in liquid PYE medium at 26°C
478 supplemented with antibiotics or supplements as necessary (kanamycin 5 µg ml^{-1},
479 gentamicin 0.5 µg ml^{-1}, spectinomycin 25 µg ml^{-1}, streptomycin 5 µg ml^{-1}, and 0.3 mM
480 diaminopimelic acid). Strains were maintained on PYE plates at 26°C supplemented
481 with antibiotics or supplements as necessary (kanamycin 5 or 20 µg ml^{-1}, gentamicin 2.5
482 µg ml^{-1}, spectinomycin 50 µg ml^{-1}, streptomycin 20 µg ml^{-1}, 3% sucrose, and 0.3 mM
483 diaminopimelic acid). For phosphate starvation, cells were grown in Hutner base-
484 imidazole-buffered-glucose-glutamate (HIGG) medium [45] containing 30 µM phosphate
485 (phosphate-limited), supplemented with biotin at 40 ng ml^{-1} and antibiotics where
486 appropriate. For microscopy of PYE grown samples, strains were inoculated in PYE
487 from colonies and grown at 26°C with shaking until mid- to late-exponential phase
488 ($OD_{600} \geq 1.0$) before imaging. For microscopy of HIGG grown, phosphate-limited
489 samples, strains were inoculated in PYE from colonies and grown at 26°C with shaking
490 until late-exponential phase. Cultures were then washed 2X with deionized distilled H_2O
491 (ddH_2O), diluted 1:20 in HIGG, and grown at 26°C with shaking for 72h before imaging.

492 *E. coli* strains used in this study grown in liquid lysogeny broth (LB) medium at 37°C (or
493 30°C for BACTH assays) supplemented with antibiotics or supplements as necessary
494 (ampicillin 100 µg ml^{-1}, kanamycin 30 µg ml^{-1}, gentamicin 15 µg ml^{-1}, spectinomycin 100
495 µg ml^{-1}, streptomycin 30 µg ml^{-1}, 0.3 mM diaminopimelic acid, and X-gal 40 µg ml^{-1}).
496 Strains were maintained on LB plates at 37°C (or 30°C for BACTH assays)
497 supplemented with antibiotics or supplements as necessary (ampicillin 100 µg ml^{-1},

498 kanamycin 25 or 50 µg ml^{-1}, gentamicin 20 µg ml^{-1}, streptomycin 30 or 100 µg ml^{-1}, 0.3
499 mM diaminopimelic acid (DAP), X-gal 40 µg ml^{-1}, and 0.5 mM IPTG).

500 Electroporation of *A. biprosthecum* was performed as previously described [46].
501 Outgrowth was performed for 8-24h at 26°C. For electroporation with replicating
502 plasmids, 100 µl of outgrowth culture was plated on PYE plates with appropriate
503 selection at dilutions of 10^1, 10^0, and 10^{-1}. For electroporation with integrating plasmids,
504 outgrowth was divided into volumes of 100, 300, and 600 µl and plated on PYE plates
505 with appropriate selection.

506 In-house stocks of chemically competent BL21IDE3 (YB1000), DAP auxotroph WM3064
507 (YB7351), XL-1 Blue (YB0041), and BTH101 (YB9171) *E. coli* cells were prepared as
508 previously described [47, 48].

509 **Recombinant DNA Methods**

510 DNA amplification, Gibson cloning, and restriction digests were performed according to
511 the manufacturer. Restriction enzymes and Gibson cloning mix were from New England
512 Biolabs. Cloning steps were carried out in *E. coli* (alpha-select competent cells, Bioline
513 or XL1-Blue, Stratagene) and plasmids were purified using Zyppy Plasmid Kits (Zymo
514 Research Corporation). Sequencing was performed by the Indiana Molecular Biology
515 Institute and Eurofins MWG Operon Technologies with double stranded plasmid or PCR
516 templates, which were purified with a DNA Clean & Concentrator kits (Zymo Research
517 Corporation). Chromosomal DNA was purified using the Bactozol Bacterial DNA
518 Isolation Kit (Molecular Research Center).

519 Plasmids were introduced into all *E. coli* strains using chemical transformation
520 according to the manufacturer's protocols. Electroporation of *A. biprosthecum* was

521 performed as previously described [46]. Outgrowth was performed for 8-24h at 26°C.
522 For electroporation with replicating plasmids, 100 µl of outgrowth culture was plated on
523 PYE plates with appropriate selection at dilutions of 10^1, 10^0, and 10^{-1}. For
524 electroporation with integrating plasmids, outgrowth was divided into volumes of 100,
525 300, and 600 µl and plated on PYE plates with appropriate selection. Mating of plasmids
526 into *A. biprosthecum* was performed using the *dap*$^-$ *E. coli* strain WM3064 (YB7351)
527 [49].

528 Allelic exchange and deletions were achieved using a two-step sucrose
529 counterselection procedure with pNPTS138/pNPTS139. Insertional fusions of eGFP
530 and mVenus were made using pGFPC-1 and pVENC-4, respectively [50]. BACTH
531 plasmids were made using the Euromedex BACTH System Kit (Euromedex Cat. No.
532 EUK001).

533 **Plasmid Construction**

534 All PCR, including insert fragments for Gibson assembly, was performed using iProof
535 High-Fidelity DNA Polymerase (Bio-Rad Laboratories, Inc., Cat. No. 1725302)
536 according to the manufacturer's instructions. All plasmids were constructed via Gibson
537 assembly using NEBuilder HiFi DNA Assembly Master Mix (New England Biolabs, Inc.,
538 Cat. No. E2621X) according to the manufacturer's instructions. Prior to use in cloning,
539 all restriction enzyme digested plasmids were treated with Calf Intestinal Alkaline
540 Phosphatase (New England Biolabs, Inc., Cat. No. M0290S) according to the
541 manufacturer's instructions. All primers for Gibson assembly were designed using
542 NEBuilder Assembly Tool (New England Biolabs, Inc.). For the *bacA* complementation
543 vector, we fused the promoter region, comprising 236 bp immediately upstream of

544 ABI_34190, to the coding region of *bacA* and placed the promoter/gene fusion on the
545 low copy plasmid pMR10. The promoter/gene fusion is placed in the opposite
546 orientation of the lacZ promoter. The restriction enzymes used are as follows for
547 pNPTS138/pNPTS139-based vectors (*Eco*RV or *Sph*I/*Nhe*I), pET28a+ (*Sal*I/*Sac*I),
548 pMR10 (*Eco*RV), pVENC-4 *(Nde*I/*Kpn*I), and BACTH plasmids (*Kpn*I/*Eco*RI).

549 **Bioinformatics**

550 Genomic and protein sequence data were obtained from the Integrated Microbial
551 Genomes (IMG) database [51]. Multiple sequence alignment of bactofilin sequences
552 was performed using Jalview [52] with a MAFFT alignment using the L-INS-i preset. The
553 *C. crescentus* $BacB_{Cc}$ protein sequence used for alignment is a translation of an open
554 reading frame in CC3022 that initiates at a downstream ATG codon, as described
555 previously [12]. The predicted structure of *A. biprosthecum* BacA (ABI_34180) was
556 modeled using SWISS-MODEL [53] with the structure of *C. crescentus* BacA (CC1872;
557 PBD code 2N3D) as a template. Alignment was then processed using the ESPript
558 server [54]. Percent identity (PID) was calculated from pairwise MAFFT alignments
559 using the L-INS-i preset. $PID = \left(\frac{\#\ identical\ positions}{\min\ (TG_A, TG_B)}\right) \times 100$, where TG_A and TG_B are the
560 sum of the number of residues and internal gap positions in sequences A and B in the
561 alignment [55].

562 **Microscopy**

563 *Light Microscopy and Fluorescence Imaging*

564 For light microscopy analysis, cells were spotted onto pads made of 1% SeaKem LE
565 Agarose (Lonza, Cat. No. 50000) in PYE and topped with a glass coverslip. When
566 appropriate, the coverslip was sealed with VALAP (vaseline, lanolin, and paraffin at a
567 1:1:1 ratio). Images were recorded with inverted Nikon Ti-E microscopes using either 1)

568 a Plan Apo 60X 1.40 NA oil Ph3 DM objective with DAPI/FITC/Cy3/Cy5 or
569 CFP/YFP/mCherry filter cubes and an iXon X3 DU885 EMCCD camera or 2) a Plan
570 Apo λ 100X 1.45 NA oil Ph3 DM objective with DAPI/FITC/Cy3/Cy5 or
571 CFP/YFP/mCherry filter cubes and a Photometrics Prime 95B sCMOS camera. Images
572 were processed with NIS Elements software (Nikon). To visualize DNA, cells were
573 grown in HIGG medium for 72h as described above. Cells were washed 1x with PYE
574 and 1 µl of cell suspension was spotted onto a coverslip and topped with an agar pad.
575 Cells were monitored via phase microscopy for ~1h to ensure they were growing and 20
576 µl of 1 mg/ml of 4',6-diamidino-2-phenylindole dihydrochloride (DAPI) was spotted on
577 top of the agar pad. DAPI was allowed to diffuse through the pad to the cells and cells
578 were imaged.

579 *Structured Illumination Microscopy*
580 3D-SIM images were collected on a DeltaVision OMX system (Applied Precision Inc.,
581 Issaquah, USA) equipped with a 1.4NA Olympus 100X oil objective. A 405 nm laser
582 source and 419-465 nm emission filter were used for collecting HADA signal. A 488 nm
583 laser source and 500-550 nm emission filter were used for collecting GFP signal. A 568
584 nm laser source and 609-654 emission filter were used for collecting TADA signal. The
585 z-axis scanning depth was 2 µm. Immersion oil with refraction index of 1.514 was used.
586 SIM images were reconstructed using softWoRx.

587 *Electron Microscopy*
588 10 µl cell or sacculi suspension was applied to an electron microscopy grid
589 (Formvar/Carbon on 300 mesh; Ted Pella Inc., Cat. No. 01753-F) for 5 min at room
590 temperature. Excess liquid was removed with Whatman filter paper. Cells or sacculi
591 were then negatively stained with 10 µl 1% uranyl acetate (UA) and excess UA liquid

592 was immediately removed with Whatman filter paper. Grids were allowed to dry, stored
593 in a grid holder in a desiccation chamber, and imaged with a kV JEOL JEM 1010
594 transmission electron microscope (JEOL USA Inc.). Protein visualization was performed
595 as sacculi suspension except protein was applied to the grid for 1 min and stained with
596 2% UA before imaging.

597 **Sacculi purification**

598 Strains were inoculated in 3 ml PYE from colonies and grown at 26°C with shaking until
599 late-exponential phase. Cultures were then washed 2X with ddH_2O, diluted 1:50 in
600 HIGG, and grown at 26°C with shaking for 72h. Cells were harvested by centrifugation
601 (7,000 g, 4°C, 15 min) and resuspended in 10 ml ddH_2O. Cell suspension was added
602 dropwise to 20 ml boiling 7.5% SDS in a 125 ml flask with a stir bar. Once cells addition
603 was complete, the SDS cell suspension was boiled for 30 min with stirring and then
604 allowed to cool to room temperature. Suspension was then washed 6X with ddH_2O
605 using centrifugation (100,000 g, 25°C, 30 min) to isolate the sacculi pellet and
606 resuspended in 5 ml ddH_2O before imaging.

607 **Protein purification**

608 Recombinant plasmids overproducing His_6-BacA protein were transformed into BL21 *E.*
609 *coli* strain. Transformants were grown, in LB medium supplemented with kanamycin (50
610 μg ml^{-1}), at 37°C until the OD_{600} = 0.6. Expression was induced by adding 0.5 mM IPTG
611 (isopropyl β-D-thiogalactopyranoside) and incubation was continued either 3h at 30°C
612 or overnight at 20°C. Cells pellets were resuspended in 1/25 volume of Buffer A
613 (TrisHCl at pH 8, 300 mM NaCl, 2 mM β-mercaptoethanol) and lysed by sonication (20
614 sec On / 40 sec Off, 5 min, Misonix S4000). Cells debris were pelleted by centrifugation
615 at 36,000 g for 30 min at 4°C. The supernatant was loaded on a Ni-NTA resin (Qiagen)

616 on an AKTA FPLC pure system. After washing with Buffer A, the protein was eluted with
617 a linear gradient of Buffer B (50 mM TrisHCl at pH 8, 300 mM NaCl, 2 mM β-
618 mercaptoethanol, 500 mM imidazole). Elution fraction was loaded on SDS page gel and
619 peak fractions containing the protein were pooled. Upon purification, His_6-BacA protein
620 was used for polymerization assay. Polymerization assay were performed by dialyzing
621 His_6-BacA in Buffer C (25 mM TrisHCl at pH 8, 250 mM NaCl, 2 mM β-mercaptoethanol)
622 supplemented with 10% Triton X-100 in the case of BacA.

623 **Western blots**

624 All strains were grown until OD=1.0 before being centrifuged and resuspended in 100 µl
625 of 1xPBS supplemented with 0.1 µl of Universal Nuclease (Pierce #88700) sonicated for
626 3 times for 10sec at 50% intensity (Misonix S4000). Protein concentration was
627 measured and normalized if needed before addition of laemmli buffer. 15 µl of each
628 sample was loaded onto 4-20% precast polyacrylamide gels (BioRad) before being
629 transferred on a nitrocellulose membrane according to manufacturer's instructions.
630 Loading was controlled by Ponceau's staining before immunoblotting was performed by
631 addition of an anti-GFP polyclonal antibody (MBL #598) as the primary antibody and a
632 goat anti-rabbit HRP (Pierce) as secondary antibody. Transferred blots were visualized
633 with SuperSignal West Pico substrate (ThermoFisher Scientific) using a Bio-Rad
634 Chemidoc.

635 **Image analysis**

636 Stalk length and stalk percentage data was obtained using FIJI (Fiji Is Just ImageJ) [56].
637 Briefly, phase micrographs were imported into FIJI and stalks were manually traced
638 using the "Freehand Line" tool. Stalks lengths were determined from the manual trace
639 using the "Measure" function, calibrated to the µm/pixel scale of the original micrograph.

640 The percentage of stalked cells per image was calculated by manually counting the
641 number of stalked and non-stalked cells per image. Subcellular localization of SpmX-
642 eGFP and BacA-mVenus foci and subsequent localization heatmaps were generated
643 using the ImageJ plugin MicrobeJ [57]. SpmX-eGFP maxima area and intensity were
644 determined using the ImageJ plugin MicrobeJ [57]. Area was first generated as pixel
645 area and converted to nm^2 based on the pixel to µm ratio for the images. Intensity is
646 defined as the average gray value measured on the channel used to detect the particle.
647 Analysis of BacA-mVenus time-lapse movies and BacA-mVenus foci dynamics was
648 performed using the ImageJ plugin TrackMate [58]. Colocalization analysis was
649 performed by using MicrobeJ [57] to detect all cells that contained both BacA-mVenus
650 and SpmX-mCherry foci and then measure colocalization by Pearson correlation
651 coefficient. All statistical analysis and data visualization was generated in R version 3.5
652 [59] and using the ggplot2 [60] and ggsignif [61] packages.

653 Cell silhouettes and cell body outlines were produced by importing the phase
654 micrograph into Adobe Illustrator CC 2015.2.1 (Adobe Inc.) and manually tracing the
655 silhouette or outline.

656

657 **Acknowledgements**
658 The NIH supported this work with grants 2R01GM051986 and R35GM122556 (to
659 Y.V.B.) and GM113172 to M.S.V. and Y.V.B. Y.V.B. is also supported by a Canada 150
660 Research Chair in Bacterial Cell Biology. Structured illumination microscopy (3D-SIM)
661 data acquisition was supported by NIH grant NIH1S10OD024988-01 to the Indiana
662 University Bloomington Light Microscopy Imaging Center.

663 **Author contributions**
664 Conceptualization, P.D.C. and Y.V.B.; Methodology, P.D.C., M.J., and Y.V.B.;
665 Investigation, P.D.C. and M.J.; Resources, Y.V.B. and fluorescent D-amino acids
666 (FDAAs) from M.S.V.; Writing – Original Draft, P.D.C; Writing – Review and Editing,
667 P.D.C., M.J., and Y.V.B.; Visualization, P.D.C.; Supervision, Y.V.B.; Funding
668 Acquisition, Y.V.B.

669 **Competing interests**
670 The authors declare no competing interests.

671 **Additional Information**
672 All bacterial mutant strains generated during this study are available from the
673 corresponding author upon request.

674

675

Table 1 – Plasmids used in this study

Plasmid	Genotype/description	Reference/source
Basic vectors		
pMR10	RK2-based, broad-host-range low copy cloning vector, Kan^R	R. Roberts and C. Mohr, unpublished
pNPTS138	sacB-containing Litmus 38 derivative suicide vector used for double homologous recombination, Kan^R	M.R.K. Alley, unpublished
pNPTS139	sacB-containing Litmus 39 derivative suicide vector used for double homologous recombination, Kan^R	M.R.K. Alley, unpublished
pGFPC-1	Integration plasmid used for creating C-terminal fusions to eGFP, $Spec/Strep^R$	[50]
pVENC-4	Integration plasmid used for creating C-terminal fusions to mVenus, $Gent^R$	[50]
pKT25	BACTH plasmid for generating in-frame fusions at the C-terminal end of the T25 fragment, Kan^R	EuroMedex
pKNT25	BACTH plasmid for generating in-frame fusions at the N-terminal end of the T25 fragment, Kan^R	EuroMedex
pUT18	BACTH plasmid for generating in-frame fusions at the N-terminal end of the T18 fragment, Amp^R	EuroMedex
pUT18C	BACTH plasmid for generating in-frame fusions at the C-terminal end of the T18 fragment, Kan^R	EuroMedex
pET28a+	His_6-tag expression vector, Kan^R	Novagen
Plasmids		
pKT25-zip	pKT25 derivative in which the leucine zipper of GCN4 yeast protein is genetically fused in frame to the T25 fragment. BACTH positive control; Kan^R	EuroMedex
pUT18C-zip	pUT18C derivative in which the leucine zipper of GCN4 yeast protein is genetically fused in frame to the T18 fragment. BACTH positive control; Amp^R	EuroMedex
pGFPC-1-$spmX_{AB}$	pGFPC-1 bearing the C-terminal fragment of *spmX* (ABI_31540); $Spec/Strep^R$	[11]
pCHYC-1-$spmX_{AB}$	pCHYC-1 bearing the C-terminal fragment of *spmX* (ABI_31540); $Spec/Strep^R$	[11]
pPC10	pNPTS139 derivative used to generate a clean deletion of *bacA* (ABI_34180); Kan^R	this study
pPC21	pVENC-4 bearing the C-terminal fragment *bacA* (ABI_34180) $_{(nt\ 44\text{-}543)}$; $Gent^R$	this study
pPC36	Δ*bacA* complementation vector; pMR10 containing the promotor region upstream of the ABI_34190/ABI_34180 loci fused to the coding region of ABI_34180; Kan^R	this study
pPC62	pKT25 derivative in which SpmX is genetically fused in-frame to the T25 fragment; Kan^R	this study
pPC63	pKT25 derivative in which BacA is genetically fused in-frame to the T25 fragment; Kan^R	this study
pPC65	pKNT25 derivative in which BacA is genetically fused in-frame to the T25 fragment; Kan^R	this study
pPC67	pUT18 derivative in which SpmX is genetically fused in-frame to the T18 fragment; Amp^R	this study
pPC68	pUT18 derivative in which BacA is genetically fused in-frame to the T18 fragment; Amp^R	this study
pPC70	pUT18C derivative in which SpmX is genetically fused in-frame to the T18 fragment; Amp^R	this study
pPC72	pKNT25 derivative in which SpmX is genetically fused in-frame to the T25 fragment; Kan^R	this study
pPC73	pUT18C derivative in which BacA is genetically fused in-frame to the T18 fragment; Amp^R	this study
pMJ2	pET28a+ derivative to overexpress His-tagged $BacA_{Cc}$ (CC_1873) in *E. coli*; Kan^R	this study
pMJ4	pET28a+ derivative to overexpress His-tagged BacA (ABI_34180) in *E. coli*; Kan^R	this study
YB8246	pNPTS138-Δ$spmX_{Ab}$; Kan^R	[15]

676

677

Table 2 – Strains used in this study

Strain	Genotype/description	Construction	Reference/source
E. coli			
DH5α Silver Select	F^- deoR endA1 recA1 relA1 gyrA96 hsdR17(n_K^-, m_K^+) supE44 thi-1 phoA Δ(lacZYA argF)U169 Φ80lacZΔM15λ⁻; Standard strain for cloning and maintaining plasmids	-	BioLine
BL21IDE3 (YB1000)	(F- ompT hsdSB (rB-mB-) gal dcm (IDE3); Used for protein overexpression.	-	Novagen
XL1-Blue (YB0041)	recA1, endA1, gyrA96, thi-1, hsdR17, supE44, relA1, lac [F' proAB, $lacI^qZ\Delta M15$, Tn10(Tet^r)]; Used for cloning and maintaining BACTH plasmids	-	Stratagene
BTH101 (YB9171)	F^-, cya-99, araD139, galE15, galK16, rpsL1 (Strr), hsdR2, mcrA1, mcrB1; Used for BACTH assays	-	EuroMedex
YB5681	DH5α strain for maintaining pGFPC-1-$spmX_{AB}$	-	[11]
YB7351	thrB1004 pro thi rpsL hsdS lacZΔM15 RP4-1360 Δ(araBAD)567 ΔdapA1341::[erm pir]; DAP (diaminopimelic acid) auxotroph used for conjugation, referred to as strain WM3064 in reference	-	[49]
YB7552	DH5α strain for maintaining pPC10	Transformation of pPC10 into DH5α	this study
YB8159	DAP auxotroph conjugative donor *E. coli* for mating plasmids into *A. biprosthecum*	Transformation of pPC10 into YB7351	this study
YB8177	DH5α strain for maintaining pPC21	Transformation of pPC21 into DH5α	this study
YB8537	DH5α strain for maintaining pMJ2	Transformation of pMJ2 into DH5α	this study
YB8539	DH5α strain for maintaining pMJ4	Transformation of pMJ4 into DH5α	this study
YB8246	DH5α strain for maintaining pNPTS138-*ΔspmX*$_{Ab}$	Transformation of pNPTS138-*ΔspmX*$_{Ab}$ into DH5α	[15]
YB8552	BL21IDE3 strain containing pMJ2. For overexpression of $BacA_{Cc}$.	Transformation of pMJ2 into YB1000	this study
YB8554	BL21IDE3 strain containing pMJ4. For overexpression of BacA.	Transformation of pMJ4 into YB1000	this study
YB8584	DH5α strain for maintaining pPC36	Transformation of pPC36 into DH5α	this study
YB9158	XL1-Blue strain for maintaining pPC62	Transformation of pPC62 into YB0041	this study
YB9159	XL1-Blue strain for maintaining pPC63	Transformation of pPC63 into YB0041	this study
YB9161	XL1-Blue strain for maintaining pPC72	Transformation of pPC72 into YB0041	this study
YB9162	XL1-Blue strain for maintaining pPC65	Transformation of pPC65 into YB0041	this study
YB9164	XL1-Blue strain for maintaining pPC67	Transformation of pPC67 into YB0041	this study
YB9165	XL1-Blue strain for maintaining pPC68	Transformation of pPC68 into YB0041	this study
YB9167	XL1-Blue strain for maintaining pPC70	Transformation of pPC70 into YB0041	this study
YB9168	XL1-Blue strain for maintaining pPC73	Transformation of pPC73 into YB0041	this study
A. biprosthecum			
YB642	*A. biprosthecum* C19	-	[62]
YB5692	C19 *spmX*::*spmX-eGFP* ($Spec^R$/$Strep^R$)	Electroporation of pGFPC-1-$spmX_{AB}$ into YB642	[11]
YB7474	C19 *bacA*::*bacA-mVenus* ($Gent^R$)	Electroporation of pPC21 into YB642	this study
YB7487	C19 Δ*spmX bacA*::*bacA-mVenus* ($Gent^R$)	Electroporation of pPC21 into YB8237	this study
YB7489	C19 Δ*bacA* Δ*spmX*	Mating of YB8237 with YB8159.	this study
YB7561	C19 *spmX*::*spmX-eGFP* Δ*bacA* ($Spec^R$/$Strep^R$)	Electroporation of pGFPC-1-$spmX_{AB}$ intoYB8597	this study
YB8237	C19 Δ*spmX*	Electroporation of plasmid from YB8246 into YB642	[15]
YB8597	C19 Δ*bacA*	Mating of YB642 with YB8159	this study
YB8601	C19 Δ*bacA* / pPC36 (Kan^R)	Electroporation of pPC36 into YB8597	this study
YB8620	C19 Δ*bacA* / pMR10 (Kan^R)	Electroporation of pMR10 into YB8597	this study
YB9183	C19 / pMR10 (Kan^R)	Electroporation of pMR10 into YB642	this study
YB9466	C19 *bacA*::*bacA-mVenus spmX*::*spmX-mCherry* ($Spec^R$/$Strep^R$)	Electroporation of pCHYC-1-$SpmX_{AB}$ plasmid into YB7474	this study
YB9521	C19 *spmX*::*spmX-eGFP* Δ*bacA* ($Spec^R$/$Strep^R$) / pPC36 (Kan^R)	Electroporation of pPC36 into YB7561	this study

678

679 **Table 3 – Primers used in this study**

Primer ID	Sequence (5' to 3')[1]	Restriction site	Purpose
ABI_34180SeqUp	CAGGCGTTGTCTCCTTTGTC	-	Sequencing the ABI_34180
ABI_34180SeqDn	CGACTGGACGGTTGAAAAGG	-	(*bacA*) locus
ABI_34190SeqUp	GTTAAACCTTGCGCCGTTCG	-	Sequencing the ABI_34190
ABI_34190SeqDn	GGCACTGCGGTTGAGATTGA	-	locus
AbiBacA500C-V4F	gagacgtccaattg**catatg**AACCGACCCCGGCTCCGC	NdeI	Generation of pPC21
AbiBacA500C-V4R	tcgagatcttaa**ggtacc**CTTCAGGTCGCCCAGAGCG	KpnI	
ABI_PlmdC-bacA_F	acgccaagcttccatgggatCTACTTCAGGTCGCCCAG	-	Generation of pPC36
AbiPlytMbacA2F	CGGCGGTTATGTTCAACAAAACTAACAAACCGG	-	
AbiPlytMbacA1R	GTTGAACATAACCGCCGCCACCTAAAC	-	
ABI_PlmdC_R	gctctgcaggagatctcgatAATGTCCTTATGCAATCC	-	
delABI34180upF	aattctggatccacgatTCAATGTCGACGAAGACTTC	-	Generation of pPC10
delABI34180upR	GAGGTGGATTAGTTTTGTTGAACATAATCTCCTG	-	
delABI34180dnF	ACAAAACTAATCCACCTCACCGAACTTAATCTGTGAAGAAAGC	-	
delABI34180dnR	aagcttcctgcaggatGCGGATTCGACCGTGCCG	-	
oMJ3_BacAcc	cga**gagctc**ATGTTCAGCAAGCAAGCTAAATCG	SacI	Generation of pMJ2
oMJ4_BacAcc	taa**gtcgac**TTAGCCGGCGCTCTTGG	SalI	
oMJ5_BacAab	aga**gagctc**ATGTTCAACAAAACTAACAAACCGG	SacI	Generation of pMJ4
oMJ6_BacAab	ata**gtcgac**CTACTTCAGGTCGCCCAG	SalI	
pUT18C_AbiSpmX-F	tctagaggatccccg**ggtacc**gGTGATGAGAGCGCGTCAAAAG	KpnI	Generation of pPC62
pKT25_AbiSpmX-R	acgttgtaaaacgacggcc**gaattc**TCAGTCCTTGAGGCCGCC	EcoRI	
pKT25_AbiBacA-F	tctagaggatccccg**ggtacc**tATGTTCAACAAAACTAACAAACC	KpnI	Generation of pPC63
pKT25_AbiBacA-R	acgttgtaaaacgacggcc**gaattc**CTACTTCAGGTCGCCCAG	EcoRI	
pKTN25_AbiBacA-F	tctagaggatccccg**ggtacc**gATGTTCAACAAAACTAACAAACCGG	KpnI	Generation of pPC65
pKTN25_AbiBacA-R	cgattgctgcatggtcatt**gaattc**gaCTTCAGGTCGCCCAGAGC	EcoRI	
pUT18C_AbiSpmX-F	tctagaggatccccg**ggtacc**gGTGATGAGAGCGCGTCAAAAG	KpnI	Generation of pPC67
pUT18_AbiSpmX-R	cgtggcctcgctggcggct**gaattc**gaGTCCTTGAGGCCGCCAAG	EcoRI	
pKTN25_AbiBacA-F	tctagaggatccccg**ggtacc**gATGTTCAACAAAACTAACAAACCGG	KpnI	Generation of pPC68
pUT18_AbiBacA-R	cgtggcctcgctggcggct**gaattc**gaCTTCAGGTCGCCCAGAGC	EcoRI	
pUT18C_AbiSpmX-F	tctagaggatccccg**ggtacc**gGTGATGAGAGCGCGTCAAAAG	KpnI	Generation of pPC70
pUT18C_AbiSpmX-R	attacttagttatatcgat**gaattc**gaTCAGTCCTTGAGGCCGCC	EcoRI	
pUT18C_AbiSpmX-F	tctagaggatccccg**ggtacc**gGTGATGAGAGCGCGTCAAAAG	KpnI	Generation of pPC72
pKTN25_AbiSpmX-R	cgattgctgcatggtcatt**gaattc**gaGTCCTTGAGGCCGCCAAG	EcoRI	
pKTN25_AbiBacA-F	tctagaggatccccg**ggtacc**gATGTTCAACAAAACTAACAAACCGG	KpnI	Generation of pPC73
pUT18C_AbiBacA-R	attacttagttatatcgat**gaattc**gaCTACTTCAGGTCGCCCAG		

680 [1]Restriction sites in **bold**; Genomic sequence in CAPS

681 **Figures**

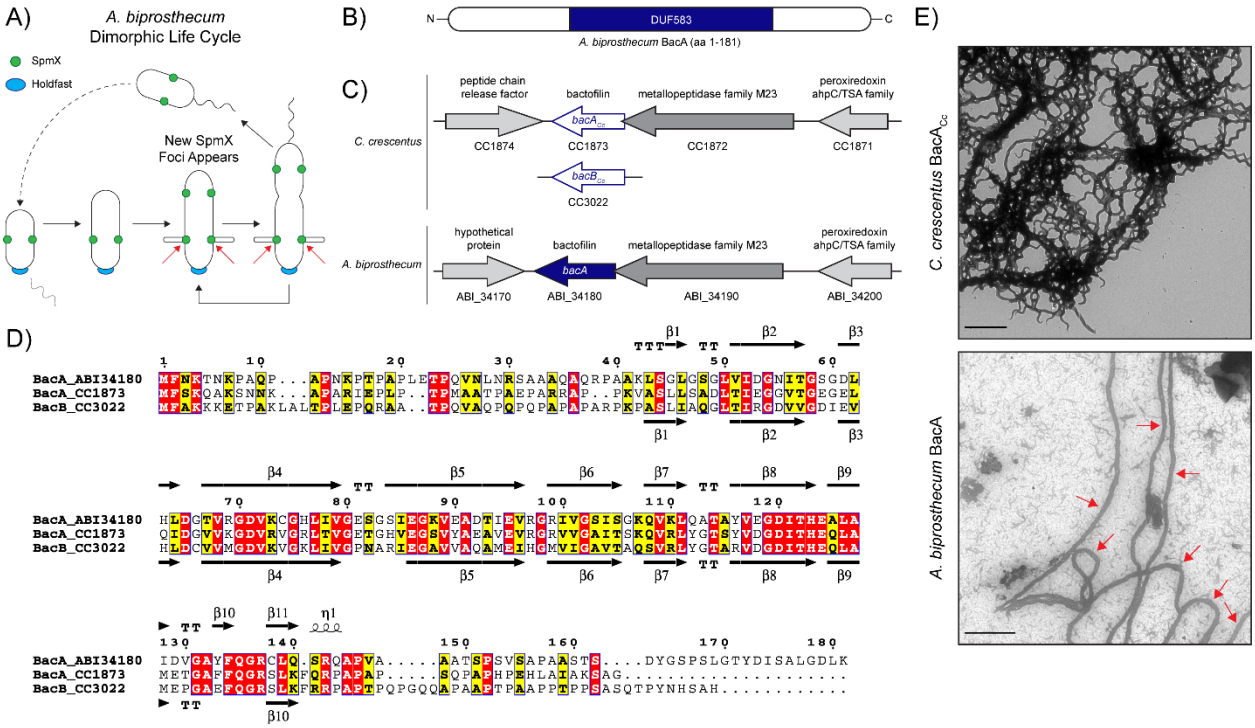

682

683 **Figure 1 – Comparison of *Caulobacter crescentus* and *Asticcacaulis biprosthecum* Bactofilins**

684 **A)** Dimorphic life cycle of *A. biprosthecum*. A common characteristic of prosthecate Alphaproteobacteria,
685 the prosthecate mother cell produces an adhesive holdfast (shown in blue) at one pole. Cell division
686 results in a motile, nonreplicating swarmer cell that differentiates into a prosthecate cell. Red arrows
687 indicate the base of *A. biprosthecum* stalks. Green circles indicate SpmX localization.

688 **B)** Schematic of the BacA protein from *A. biprosthecum*. The conserved bactofilin (DUF583) domain is
689 shown in blue.

690 **C)** Schematics of the bactofilin gene loci for both *C. crescentus* and *A. biprosthecum*.

691 **D)** Alignment of *A. biprosthecum* BacA (ABI_34180) and *C. crescentus* $BacA_{Cc}$/$BacB_{Cc}$
692 (CC1873/CC3022). Conserved residues are shown in red boxes, similar residues in yellow boxes with
693 bold characters. The secondary structure of *A. biprosthecum* BacA ("BacA_ABI34180") was modeled
694 using the SWISS-MODEL server [53] with the structure of *C. crescentus* $BacA_{Cc}$ ("BacA_1873"; PBD
695 code 2N3D) as a template [63]. The secondary structures of *C. crescentus* $BacA_{Cc}$ (PDB code 2N3D) and
696 the predicted ones for *A. biprosthecum* BacA are indicated below and above the sequence alignment,
697 respectively. Residues are numbered according to *A. biprosthecum* BacA.

698 **E)** Transmission electron microscopy (TEM) of BacA protofilament bundles from *C. crescentus* taken in
699 detergent free conditions (top) and *A. biprosthecum* taken in the presence of 10% Triton X-100 (bottom).

700 To distinguish from background, red arrows indicate *A. biprosthecum* BacA protofilaments. Scale bars = 1
701 μm.

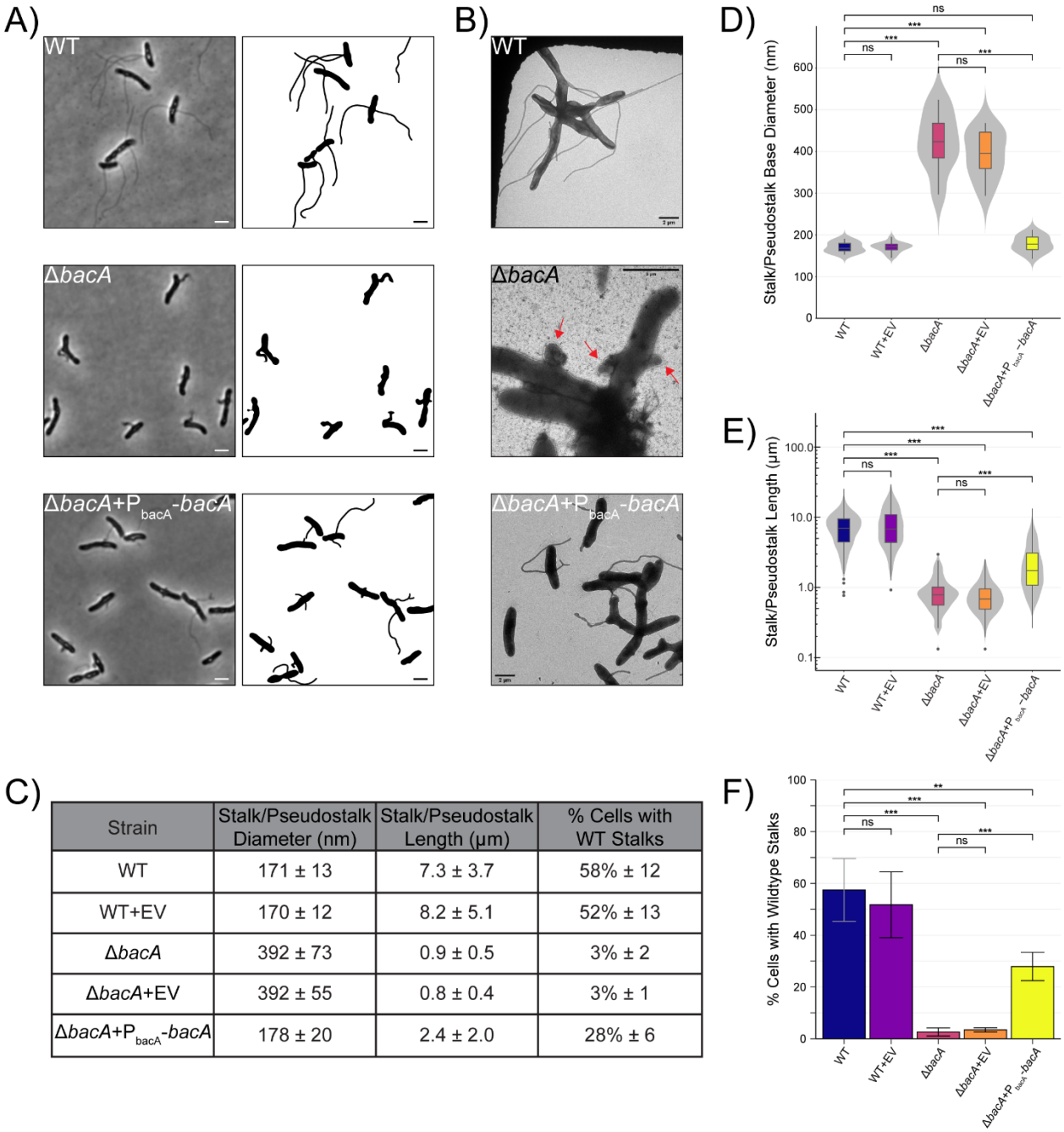

C)

Strain	Stalk/Pseudostalk Diameter (nm)	Stalk/Pseudostalk Length (µm)	% Cells with WT Stalks
WT	171 ± 13	7.3 ± 3.7	58% ± 12
WT+EV	170 ± 12	8.2 ± 5.1	52% ± 13
Δ*bacA*	392 ± 73	0.9 ± 0.5	3% ± 2
Δ*bacA*+EV	392 ± 55	0.8 ± 0.4	3% ± 1
Δ*bacA*+P_{bacA}-*bacA*	178 ± 20	2.4 ± 2.0	28% ± 6

Figure 2 – BacA is Required for WT Stalk Synthesis. Analysis of stalk morphology in strains YB642 (WT), YB9183 (WT + pMR10 empty vector control), YB8597 (Δ*bacA*), YB8620 (Δ*bacA* + pMR10 empty vector control), and YB8601 (Δ*bacA* + pMR10-P_{bacA}-*bacA*). Cells were grown in rich medium (PYE) to saturation and sub-cultured into phosphate limited (HIGG) medium at 26°C for 72h (see Methods).

A) Phase microscopy (left) and cell silhouette (right) for strains YB642 (WT), YB8597 (Δ*bacA*), and YB8601 (Δ*bacA* + pMR10-P_{bacA}-*bacA*). Scale bars = 2 µm.

709 **B)** Transmission electron microscopy (TEM) for strains YB642 (WT), YB8597 (Δ*bacA*), and YB8601
710 (Δ*bacA*+pMR10-P_{bacA}-*bacA*). Δ*bacA* pseudostalks are indicated with red arrows. Scale bars = 2 μm.

711 **C)** Summary statistics for data presented in Figure 2D, 2E, and 2F. Data shown is mean (SD).

712 **D)** Distribution of stalk/pseudostalk base diameter in the populations. Data (WT n=13; WT+EV n=19;
713 Δ*bacA* n=8; Δ*bacA*+EV n=13; Δ*bacA*+P_{bacA}-*bacA* n= 17) are from single samples with five TEM fields per
714 sample. Data are represented as box and whisker plots [64] where the middle line represents the median,
715 the lower and upper hinges correspond to the first and third quartiles (the 25th and 75th percentiles), and
716 the upper whisker extends from the hinge to the largest value no further than 1.5 * IQR from the hinge
717 (where IQR is the inter-quartile range, or distance between the first and third quartiles). The lower whisker
718 extends from the hinge to the smallest value at most 1.5 * IQR of the hinge. Data beyond the end of the
719 whiskers are called "outlying" points and are plotted individually. A mirrored density violin plot [65] is
720 underlaid to show the continuous distribution of the data. Violin plots have been scaled to the same width.
721 (***$p \leq 0.001$, ns = not significant; two-sided t-test).

722 **E)** Distribution of stalk/pseudostalk lengths in the populations, measured from the tip of the structure to
723 the cell body. Data (WT n=412; WT+EV n=321; Δ*bacA* n=153; Δ*bacA*+EV n=148; Δ*bacA*+P_{bacA}-*bacA*
724 n=324) are from three independent biological replicates with five phase microscopy fields per replicate.
725 Data are plotted on a log10 scale y-axis and are represented as box and whisker plots and violin plots in
726 the same manner as Figure 2D. As length data are approximately log-normally distributed, significant
727 difference testing was performed on log10 transformed data (***$p \leq 0.001$, ns = not significant; two-sided
728 t-test).

729 **F)** Percentage of cells with WT stalks. Cells in phase images from Figure 2A were scored as having a WT
730 stalk (i.e. a thin extension from the cell body). Cells exhibiting thick and aberrant pseudostalks were
731 excluded. Data (total cells counted: WT n=735; WT+EV n=615; Δ*bacA* n=841; Δ*bacA*+EV n=1259;
732 Δ*bacA*+P_{bacA}-*bacA* n=831) are from four independent biological replicates with five phase microscopy
733 fields per replicate. Data are represented as the mean (SD) percentage of cells with stalks. (***$p \leq 0.001$,
734 **$p \leq 0.01$, ns = not significant > 0.05; two-sided t-test).

735

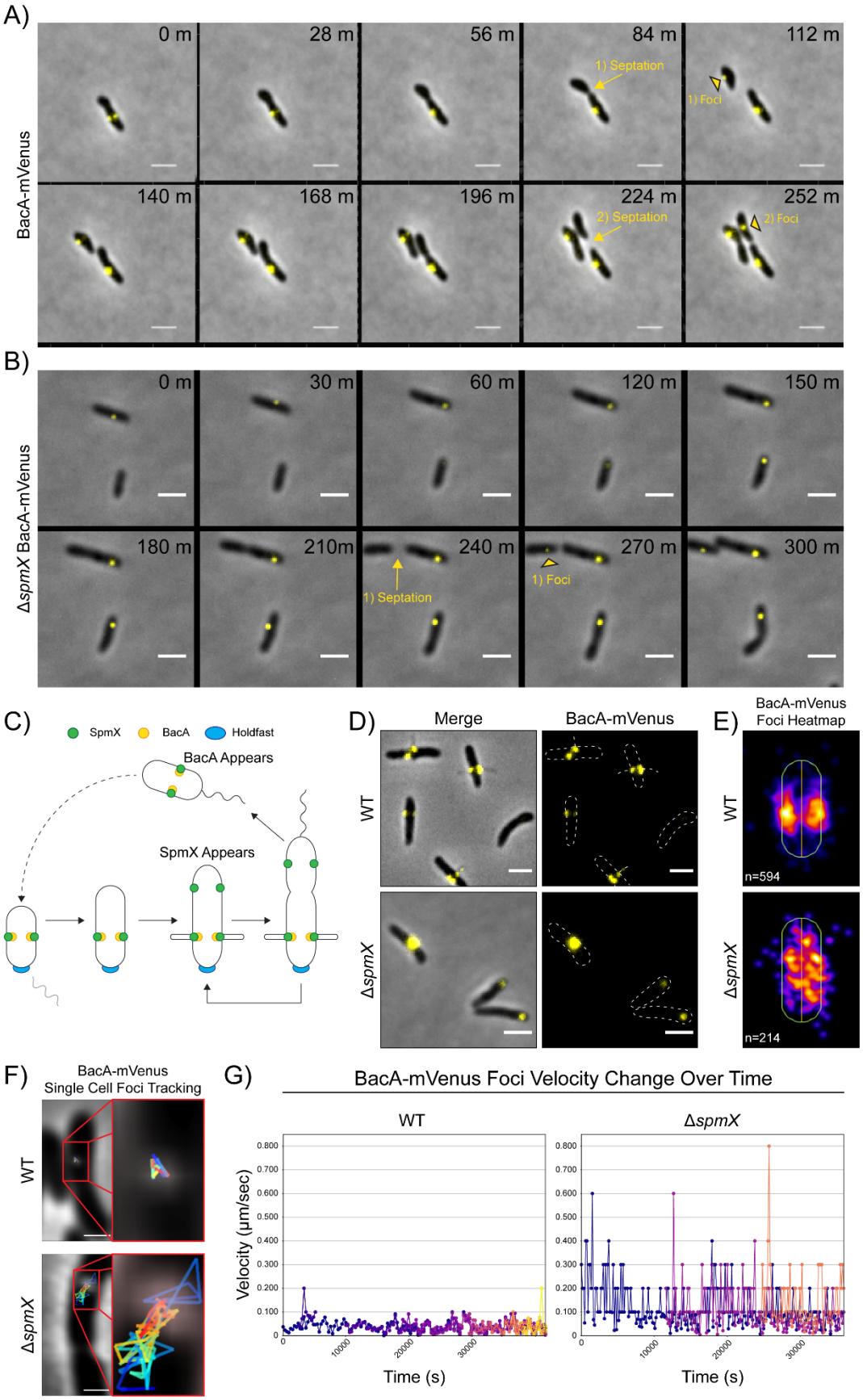
A)
BacA-mVenus
0 m
28 m
56 m
84 m
1) Septation
112 m
1) Foci
140 m
168 m
196 m
224 m
2) Septation
252 m
2) Foci
B)
ΔspmX BacA-mVenus
0 m
30 m
60 m
120 m
150 m
180 m
210m
240 m
1) Septation
270 m
1) Foci
300 m
C)
SpmX
BacA
Holdfast
BacA Appears
SpmX Appears
D)
Merge
BacA-mVenus
WT
ΔspmX
E)
BacA-mVenus
Foci Heatmap
WT
n=594
ΔspmX
n=214
F)
BacA-mVenus
Single Cell Foci Tracking
WT
ΔspmX
G)
BacA-mVenus Foci Velocity Change Over Time
WT
ΔspmX
Velocity (µm/sec)
Time (s)
Time (s)

736

737 **Figure 3 –BacA Localizes After Cell Division, Localizes to the Base of Stalks, and Requires SpmX**
738 **for Localization.** Subcellular localization of BacA-mVenus in strains YB7474 (*bacA*::*bacA-mVenus*) and
739 YB7487 (Δ*spmX bacA*::*bacA-mVenus*) grown in rich medium (PYE) at 26°C for 24-48h.

740 **A-B)** Time lapse microscopy montage showing the dynamics of BacA-mVenus localization in **A)** strain
741 YB7474 (*bacA*::*bacA-mVenus*) or **B)** strain YB7487 (*bacA*::*bacA-mVenus* Δ*spmX*). Yellow arrows and
742 text show the transition from pre-septation to post-septation. Yellow black-bordered triangles mark the
743 appearance of new BacA-mVenus foci in recently divided daughter cells. Septation events and the
744 corresponding foci appearance are numbered. Frames show images taken every **A)** 28 minutes or **B)** 30
745 minutes. Scale bars = 2 μm

746 **C)** Dimorphic life cycle of *A. biprosthecum*. The prosthecate mother cell produces an adhesive holdfast
747 (shown in blue) at one pole. Cell division results in a motile, nonreplicating swarmer cell that differentiates
748 into a prosthecate cell. Green circles indicate SpmX localization. Yellow circles indicate BacA localization.

749 **D)** BacA-mVenus subcellular localization. Phase merge and fluorescence microscopy images. Scale bars
750 = 2 μm.

751 **E)** Population level heatmaps of BacA-mVenus subcellular localization. Number of foci analyzed is shown
752 on the bottom left of each heatmap.

753 **F)** Single cell BacA-mVenus foci tracking. Tracks are colored by time, with blue representing the earliest
754 timepoints and red representing the latest time points. Scale bars = 1 μm.

755 **G)** Velocity tracking of multiple BacA-mVenus foci from time-lapse movies. Particle tracking was
756 performed and velocity (μm/s) from frame-to-frame for each focus was calculated. Each color represents
757 the track of individual foci as they appear.

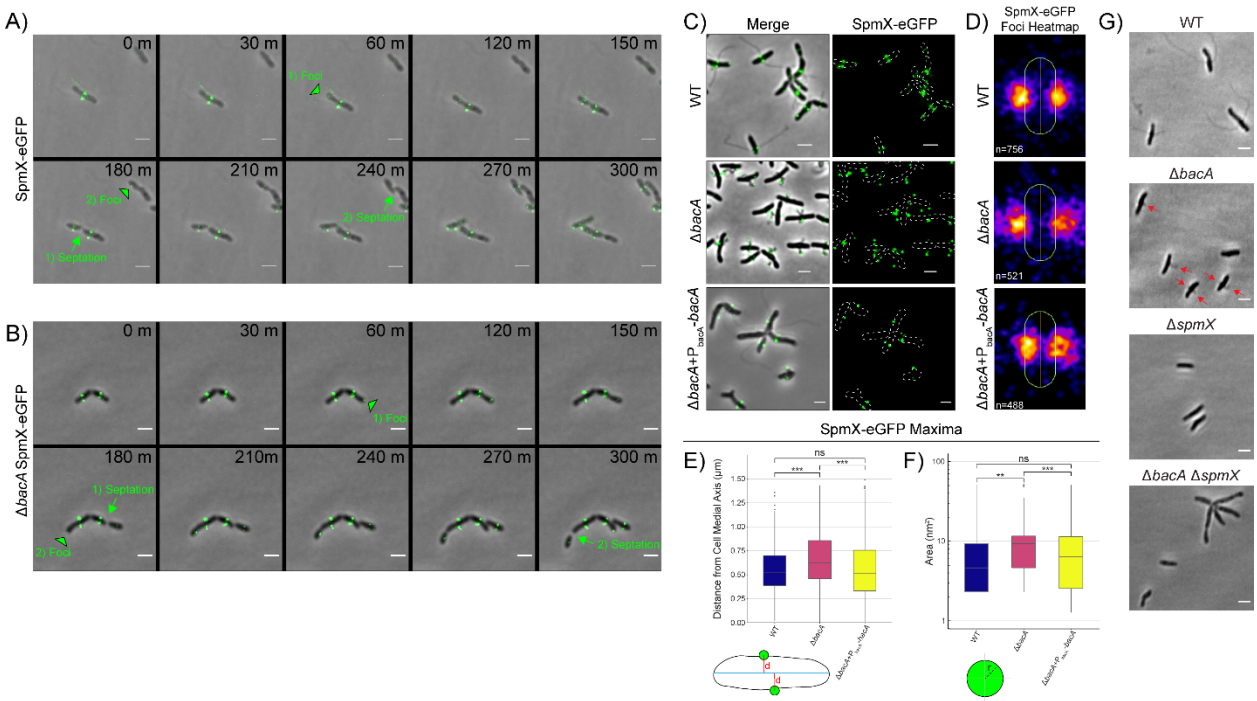

Figure 4 – BacA is not Required to Localize SpmX-eGFP, but is Required to Constrain SpmX-eGFP at the Base of the Stalk and to Constrain the Size of SpmX-eGFP Maxima.

A-B) Time lapse microscopy montage showing the dynamics of SpmX-eGFP localization in **A)** strain YB5692 (*spmX*::*spmX-eGFP*) or **B)** strain YB7561 (*spmX*::*spmX-eGFP* Δ*bacA*). Green black-bordered triangles mark the appearance of new SpmX-eGFP foci in predivisional daughter cells. Green arrows and text show the transition from pre-septation to post-septation. Foci appearance and the corresponding septation events are numbered. Frames show images taken every 30 minutes. Scale bars = 2 µm.

C) Phase merge and fluorescence microscopy images. Scale bars = 2 µm. Subcellular localization of SpmX-eGFP in strains YB5692 (*spmX*::*spmX-eGFP*; top row), YB7561 (*spmX*::*spmX-eGFP* Δ*bacA*; bottom row), and YB9521 (*spmX*::*spmX-eGFP* Δ*bacA*+P_{bacA}-*bacA*). Cells were grown in rich medium (PYE) to saturation and sub-cultured into phosphate limited (HIGG) medium at 26°C for 72h (see Methods)

D) Population level heatmaps of SpmX-eGFP subcellular localization. Number of foci analyzed is shown on the bottom left of each heatmap.

E) Distribution of orthogonal distance (µm) of each SpmX-eGFP maxima from the medial axis of its associated parent cell. Data set is the same as used in Figure 4D. Data are plotted on a continuous y-axis and are represented as box and whisker plots as described in Figure 2D. (***$p \leq 0.001$, ns = not significant > 0.05; two-sided t-test).

777 **F)** Distribution of SpmX-eGFP maxima area (nm^2) in the populations. Data set is the same as used in
778 Figure 4D. Data are plotted on a log_{10} scale y-axis and are represented as box and whisker plots as
779 described in Figure 2D. (***$p \leq 0.001$, **$p \leq 0.01$, ns = not significant > 0.05; two-sided t-test).

780 **G)** A Δ*bacA* Δ*spmX* Double Mutant Phenocopies a Δ*spmX* Single Mutant. Representative phase images
781 of YB642 (WT), YB8597 (Δ*bacA*), YB8237 (Δ*spmX*), and YB7489 (Δ*bacA* Δ*spmX*). Cells were grown in
782 rich medium (PYE) to saturation and sub-cultured into phosphate limited (HIGG) medium at 26°C for 48h-
783 72h (see Methods) before imaging. WT cells produce stalks (top left), Δ*bacA* cells produce pseudostalks
784 (top right, red arrows), and both Δ*spmX* and Δ*bacA* Δ*spmX* cells are stalkless (bottom). Scale bars = 2
785 μm.

786

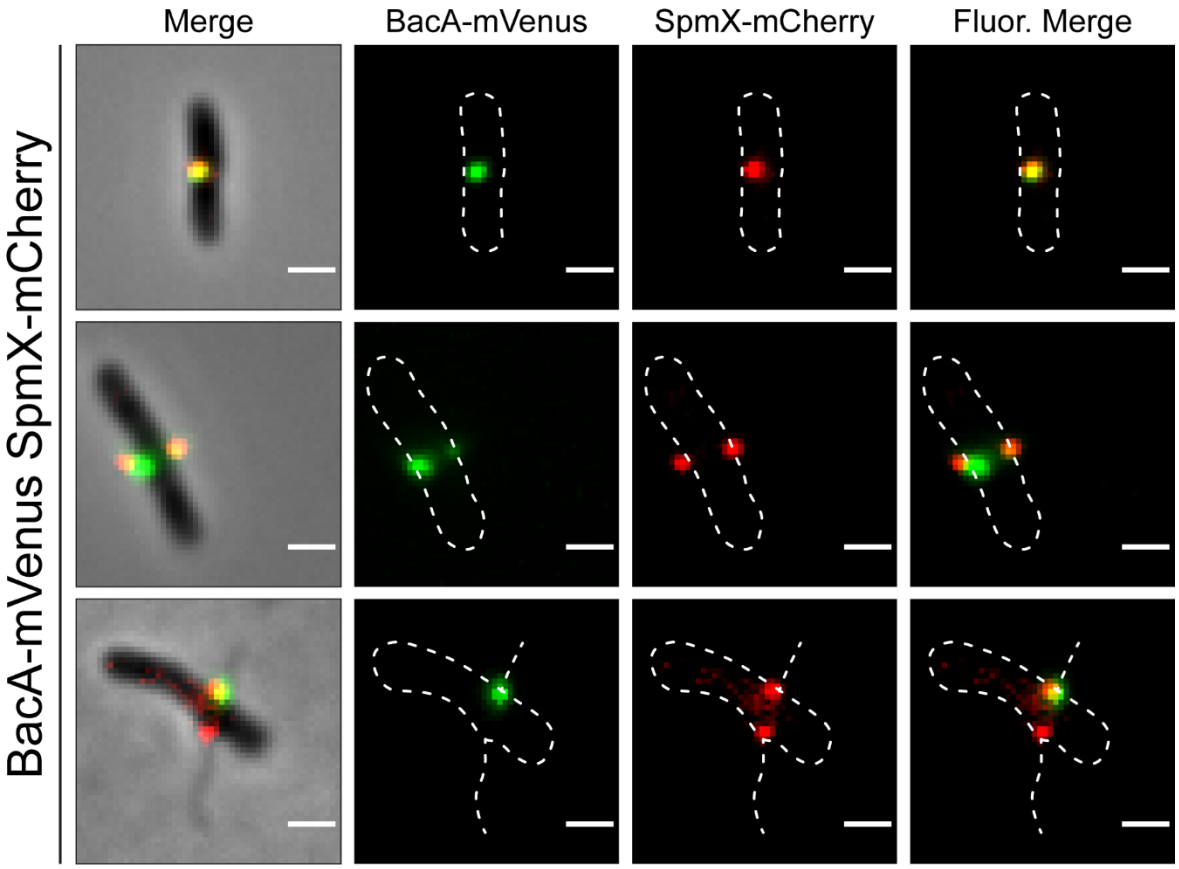

Figure 5 – BacA-mVenus and SpmX-mCherry *in vivo* Colocalization.

Representative images of dual labeled strain YB9466 (*bacA*::*bacA-mVenus spmX*::*spmX-mCherry*), with a cell exhibiting almost complete overlap of signals (top), a cell exhibiting BacA-mVenus and SpmX-mCherry foci at both putative sites of stalk synthesis (middle), and a cell with WT stalks, showing functionality of the fusion proteins (bottom).

Pearson's Correlation Coefficient (PCC) was used to quantify colocalization of signal intensity between the two fluorophore channels (BacA-mVenus and SpmX-mCherry) within the cells. PCC values range from -1 indicating a strong negative correlation (anticolocalization) to +1 indicating a strong positive correlation (colocalization), with a value of 0 indicating no correlation (noncolocalization). Only cells that contained both BacA-mVenus and SpmX-mCherry foci located at the midcell were used (n = 179). Mean (SD) PCC = 0.48 ± 0.23, showing an overall positive correlation.

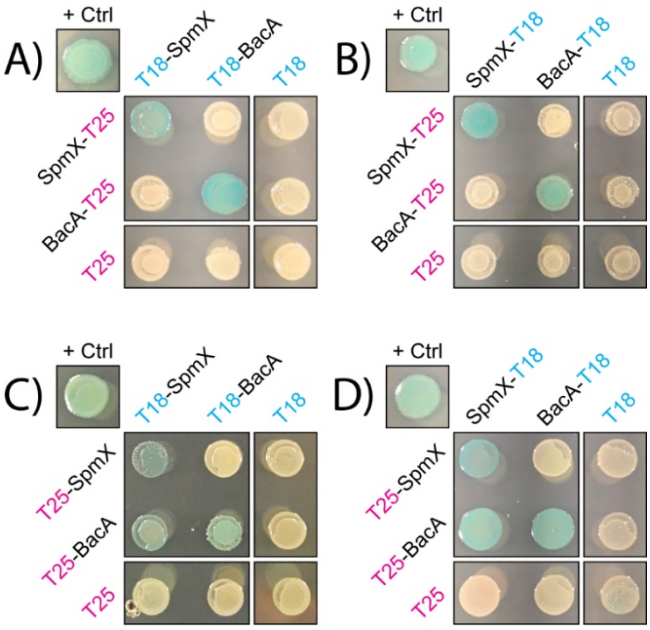

Figure 6 – Bacteria Adenylate Cyclase Two-Hybrid (BACTH) Assays Showing *in vivo* Interaction of SpmX and BacA. BTH101 *E. coli* were co-transformed with T25 and T18 based recombinant plasmids. Transformants were then grown in selective medium containing 0.5 mM IPTG and patched on selective indicator plates containing X-gal 40 µg ml^{-1} and 0.5 mM IPTG for ~24 hours at 30°C (see Methods). As this is a β-galactosidase assay, blue patches indicate a positive *in vivo* interaction between the two recombinant proteins. Positive control ("+ Crtl") for all assays is T25-Zip and T18-Zip fusion proteins. Negative controls are unfused T18 or T25 fragments in combination with the experimental fusion protein or the cognate unfused T25 or T18 fragments. Patches shown are representative of independent biological triplicates for each combination.

A) C-terminal fused T25 + N-terminal fused T18

B) C-terminal fused T25 + C-terminal fused T18

C) N-terminal fused T25 + N-terminal fused T18

D) N-terminal fused T25 + C-terminal fused T18

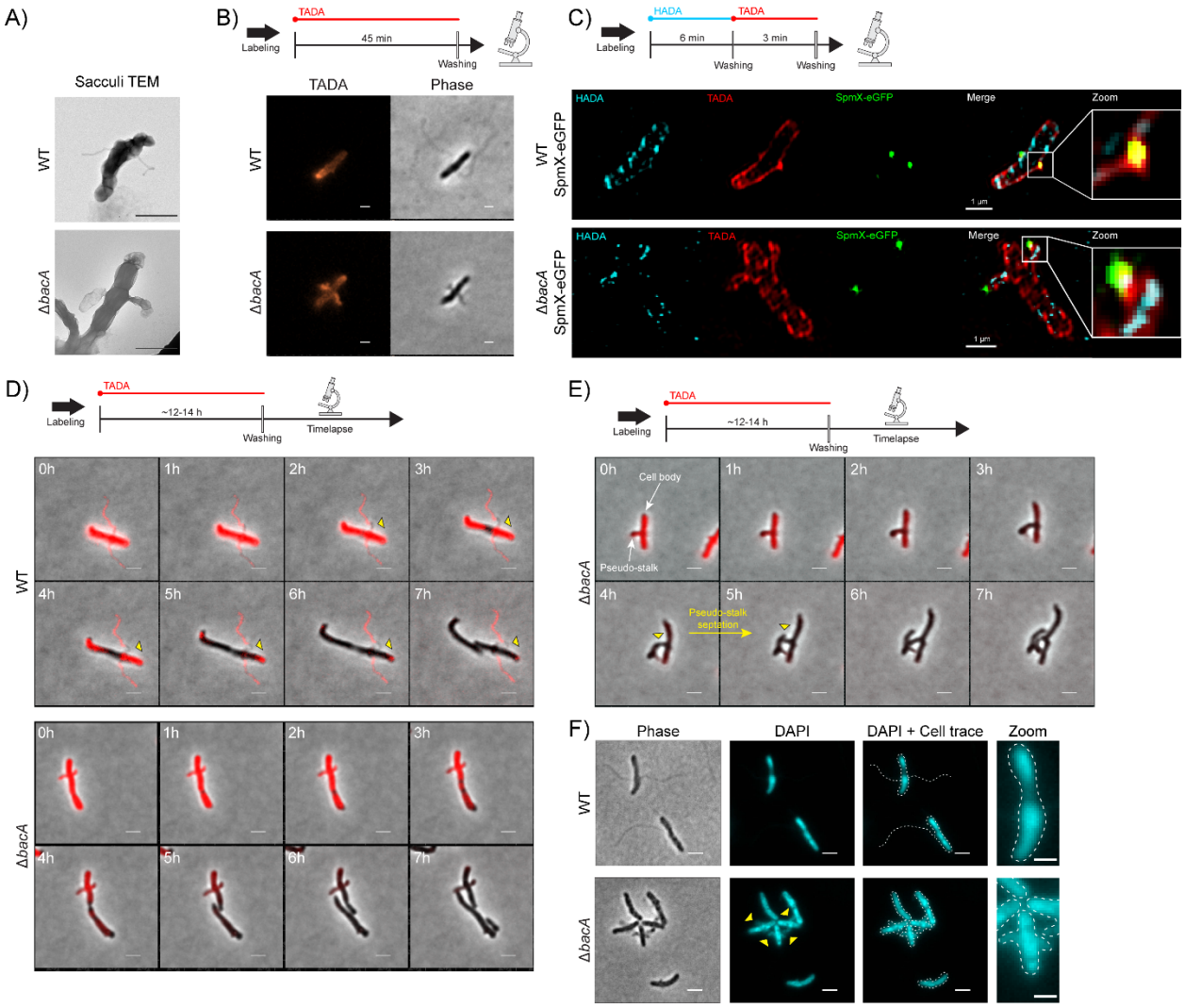

Figure 7 – Peptidoglycan (PG) Composition & Remodeling and Septation & DNA Content in WT Stalks and Δ*bacA* Pseudostalks.

A) Transmission electron microscopy (TEM) of prepared PG sacculi for strains YB642 (WT) and YB8597 (Δ*bacA*). Cells were grown in rich medium (PYE) to saturation and sub-cultured into phosphate limited (HIGG) medium at 26°C for 72h (see Methods) before preparing sacculi. Sacculi were prepared by boiling in SDS for 30 minutes followed by washing ≥6X with dH_2O. Scale bars = 1 µm

B) Medium pulse FDAA (TADA) labeling showing active PG remodeling in strains YB642 (WT) and YB8597 (Δ*bacA*). Cells were grown in rich medium (PYE) to saturation and sub-cultured into phosphate limited (HIGG) medium at 26°C for 72h (see Methods) before labeling. Cells were washed with 2X PYE, labeled with 500 µM TADA for 45 minutes, washed 2X with PYE, and imaged with phase and fluorescence microscopy. Representative images are shown. Scale bars = 2 µm.

C) Virtual time lapse: Short pulse, sequential, dual FDAA (TADA and HADA) labeling showing active PG remodeling in strains YB5692 (*spmX*::*spmX-eGFP*) and YB7561 (*spmX*::*spmX-eGFP* Δ*bacA*). Cells were

828 grown in rich medium (PYE) to saturation and sub-cultured into phosphate limited (HIGG) medium at
829 26°C for 72h (see Methods) before labeling. Cells were washed 2X with PYE, labeled with 500 μM HADA
830 for 6 minutes, washed 2X with PYE, labeled with 500 μM TADA for 3 minutes, washed 2X with PYE, and
831 imaged via 3D-SIM (Structured Illumination Microscopy). Representative images are shown. Scale bars =
832 1 μm.

833 **D)** Pulse-chase time-lapse of FDAA (TADA) labeling for strains YB642 (WT) and YB8597 (Δ*bacA*)
834 showing loss of labeling as peptidoglycan is actively remodeled. Yellow triangles with black outline
835 indicate loss of TADA signal in YB642 (WT) as stalk is extended from the base. Cells were grown in rich
836 medium (PYE) to saturation and sub-cultured into phosphate limited (HIGG) medium at 26°C for 60h (see
837 Methods) before labeling. To label whole cells, 250 μM TADA was added and cells were allowed to grow
838 an additional ~12-14h (overnight). Cells were then washed 2X with PYE to remove TADA and imaged via
839 time-lapse with phase and fluorescence microscopy. Scale bars = 2 μm.

840 **E)** Pulse-chase time-lapse of FDAA (TADA) labeling for strains YB8597 (Δ*bacA*) showing elongation and
841 septation of a pseudo-stalk. Yellow triangles with black outline indicate the septation site. Cells were
842 grown as described in Figure 6D. Scale bars = 2 μm.

843 **F)** DAPI staining for DNA in strains YB642 (WT) and YB8597 (Δ*bacA*) showing DNA is present in the
844 pseudo stalk (yellow triangles). Representative images are shown. Scale bars = 2 μm.

845

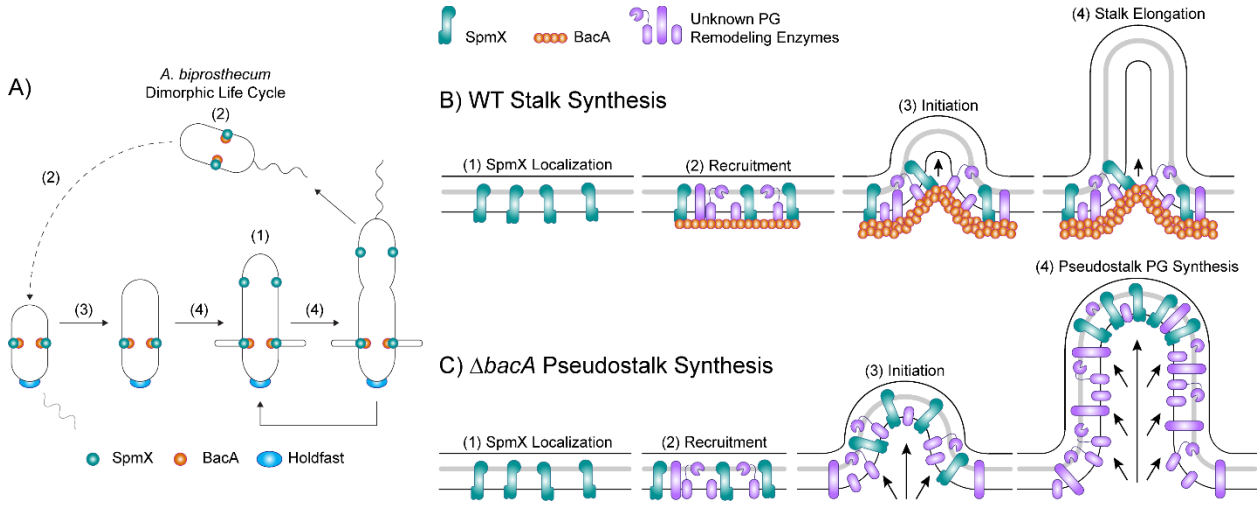

Figure 8 – Model of the Stalk PG Biosynthetic Complex in *A. biprosthecum*.

A) Dimorphic life cycle of *A. biprosthecum*. The prosthecate mother cell produces an adhesive holdfast (shown in blue) at one pole. Cell division results in a motile, nonreplicating swarmer cell that differentiates into a prosthecate cell. Green circles indicate SpmX localization. Orange circles represent BacA localization. Numbers in parentheses, (1)-(4), indicate stages of WT stalk synthesis as described in Figure 8B.

B) Model of *A. biprosthecum* WT stalk synthesis. (1) SpmX appears early in the cell cycle, prior to cell division, where it marks the future site of stalk synthesis. (2) SpmX recruits the putative PG remodeling complex and the BacA scaffold to the site of stalk synthesis. (3) PG synthesis is initiated at the site defined by SpmX localization and in an area constrained by BacA. (4) As PG synthesis progresses and the stalk elongates, synthesis is constrained at the base of the stalk by the BacA scaffold. Timing of these stages in the cell cycle are indicated by the matching numbers in Figure 8A.

C) Model of *A. biprosthecum ΔbacA* pseudostalk synthesis. As with WT cells, (1) SpmX appears early in the cell cycle, prior to cell division, where it marks the future site of stalk synthesis. (2) SpmX recruits the putative PG remodeling complex, but without BacA. (3) PG synthesis is initiated at the site defined by SpmX localization. (4) As PG synthesis progresses, there is no BacA scaffold to constrain the complex at the base of the synthesis site; PG synthesis occurs promiscuously throughout, with SpmX localized to the distal end of the structure, leading to short, wide pseudostalks. Timing of these stages in the cell cycle are indicated by the matching numbers in Figure 8A.

Protein	*C. crescentus*		*A. biprosthecum*	
	Role in stalk synthesis	Loss of function phenotype	Role in stalk synthesis	Loss of function phenotype
BacA [12]	• Cytoskeletal protein • Localizes PbpC to stalked pole	• Shorter stalks under phosphate starvation • PbpC does not localize	Unknown at time of study initiation	Unknown at time of study initiation
BacB [12]	• Cytoskeletal protein • Localizes PbpC to stalked pole	• Shorter stalks under phosphate starvation • PbpC does not localize	No homolog	N/A
PbpC [12, 27]	• Class A (bifunctional) PBP • Localizes StpX to stalked pole	• Shorter stalks under phosphate starvation • StpX does not localize	No homolog	N/A
StpX [26, 27]	• Potential role in metal homeostasis	• Shorter stalks under phosphate starvation	No homolog	N/A
SpmX [11, 36]	• None (involved in regulation of asymmetric cell division)	• Division defects	• Required for stalk synthesis • Marks site of stalk synthesis	• Stalkless cells

867

868 **Supplemental Table 1 – Proteins involved in stalk synthesis.** At the time this study was initiated, four
869 *C. crescentus proteins* (BacA, BacB, PbpC, and StpX) had been shown to be involved in stalk synthesis.
870 Of these four, only one (BacA) had a bi-directional best hit homolog in *A. biprosthecum*. The one *A.*
871 *biprosthecum* protein involved in stalk synthesis (SpmX) has a *C. crescentus* homolog, but in *C.*
872 *crescentus* this protein is involved in cell cycle regulation and not stalk synthesis.

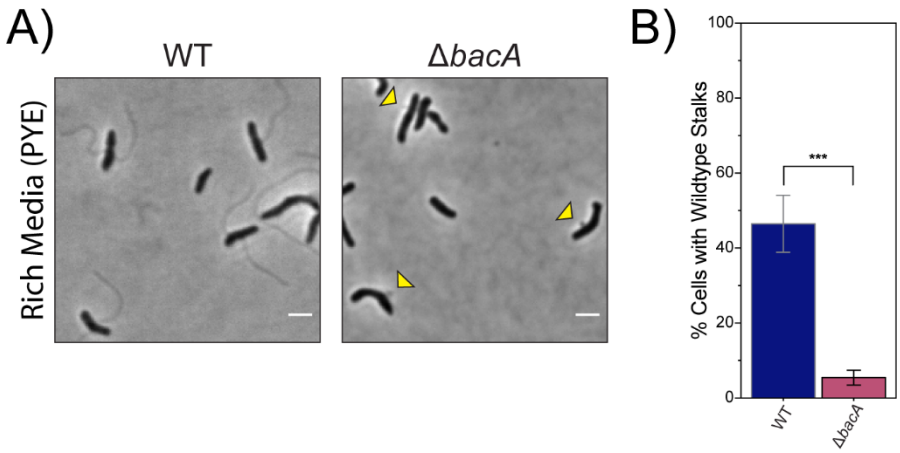

873

874 **Supplemental Figure 1 – *A. biprosthecum* stalk phenotypes in rich medium (PYE).** Analysis of stalk
875 phenotype in strains YB642 (WT) and YB8597 (Δ*bacA*). Cells were grown in rich medium (PYE) at 26°C
876 for 48h.

877 **A)** Phase microscopy for strains YB642 (WT) and YB8597 (Δ*bacA*). Scale bars = 2 µm.

878 **B)** Percentage of cells with WT stalks. Cells in phase images from Figure S1A were scored as having a
879 WT stalk (i.e. a thin extension from the cell body). Yellow triangles indicate Δ*bacA* midcell protrusions.
880 Data (total cells counted: WT n=747; Δ*bacA* n=577) are from four independent biological replicates with
881 five phase microscopy fields per replicate. Data are represented as the mean (SD) percentage of cells
882 with stalks. (***$p \leq 0.001$; two-sided t-test)

883

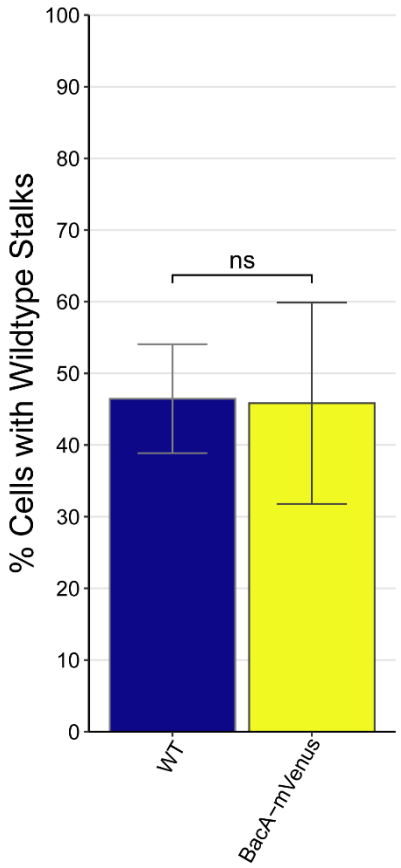

884

885 **Supplemental Figure 2 – *A. biprosthecum* BacA-mVenus is Functional.** Percentage of cells with WT
886 stalks YB642 (WT) and YB7474 (*bacA*::*bacA*-mVenus). Cells were grown in rich medium (PYE) at 26°C
887 for 48h. Data (total cells counted: WT n=747; *bacA*::*bacA*-mVenus n=378) are from four independent
888 biological replicates with five phase microscopy fields per replicate. Data are represented as the mean
889 (SD) percentage of cells with stalks. (ns = not significant > 0.05; two-sided t-test)

890

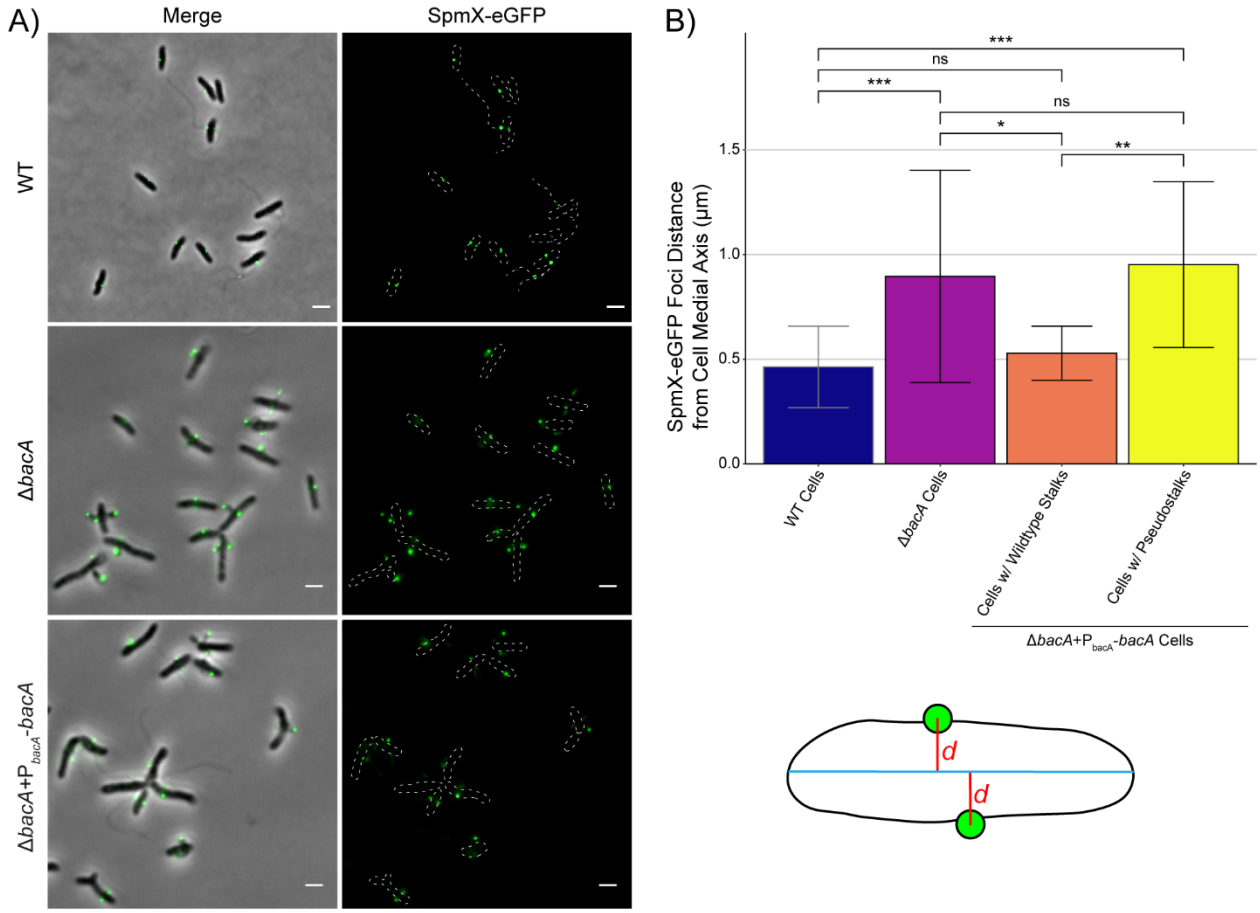

Supplemental Figure 3 – SpmX Localization is Rescued for Wildtype Stalk Synthesis when BacA Is Expressed in a Δ*bacA* background.

A) Subcellular localization of SpmX-eGFP in starins YB5692 (*spmX*::*spmX-eGFP*), YB7561 (*spmX*::*spmX-eGFP* Δ*bacA*), and YB9521 (*spmX*::*spmX-eGFP* Δ*bacA* + pMR10-P_{bacA}-*bacA*) grown in rich medium (PYE) to saturation and sub-cultured into phosphate limited (HIGG) medium at 26°C for 72h. Phase merge and fluorescence microscopy images. Scale bars = 2 µm.

B) Distribution of orthogonal distance (µm) of each SpmX-eGFP maxima from the medial axis of its associated parent cell. In order to distinguish cells with wildtype stalks from cells with pseudostalks, analysis was performed on a subset of the data presented in Figure 4C-4F. Data (WT n=49; Δ*bacA* n=22; Δ*bacA*+P_{bacA}-*bacA* n= 15) are plotted on a continuous y-axis and are represented as box and whisker plots as described in Figure 2D. (***$p \leq 0.001$, **$p \leq 0.01$, *$p \leq 0.05$, ns = not significant > 0.05; two-sided t-test).

905

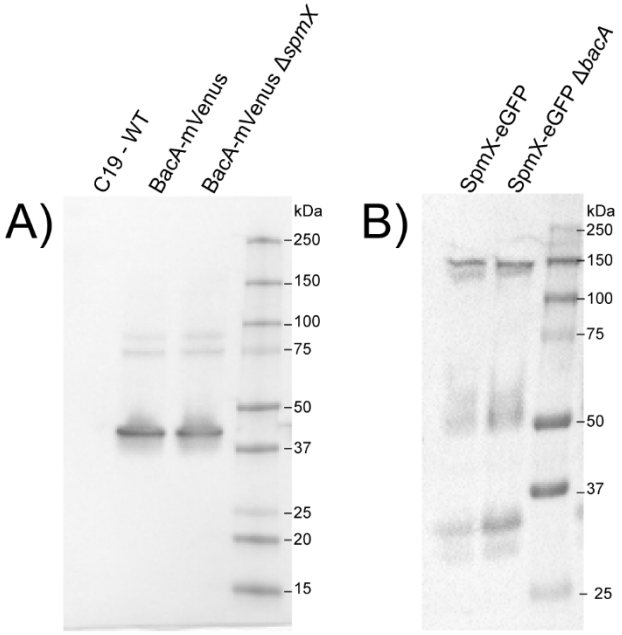

906

907 **Supplemental Figure 4 – Fluorescent Proteins are Expressed at Similar Levels in WT Cells and**
908 **Deletion Strains.**

909 **A)** Western blot against BacA-mVenus inserted at the *bacA* locus in WT (YB7474) and Δ*spmX* (YB7487)
910 cells.

911 **B)** Western blot against SpmX-eGFP inserted at the *spmX* locus in WT (YB5692) and Δ*bacA* (YB7561)
912 cells.

913 **References**

914 1. Young, K.D. (2006). The selective value of bacterial shape. Microbiol Mol Biol
915 Rev *70*, 660-703.

916 2. Justice, S.S., Hunstad, D.A., Cegelski, L., and Hultgren, S.J. (2008).
917 Morphological plasticity as a bacterial survival strategy. Nature reviews.
918 Microbiology *6*, 162-168.

919 3. Caccamo, P.D., and Brun, Y.V. (2018). The Molecular Basis of Noncanonical
920 Bacterial Morphology. Trends in microbiology *26*, 191-208.

921 4. Horvath, D.J., Jr., Li, B., Casper, T., Partida-Sanchez, S., Hunstad, D.A.,
922 Hultgren, S.J., and Justice, S.S. (2011). Morphological plasticity promotes
923 resistance to phagocyte killing of uropathogenic *Escherichia coli*. Microbes Infect
924 *13*, 426-437.

925 5. Perez-Nunez, D., Briandet, R., David, B., Gautier, C., Renault, P., Hallet, B.,
926 Hols, P., Carballido-Lopez, R., and Guedon, E. (2011). A new morphogenesis
927 pathway in bacteria: unbalanced activity of cell wall synthesis machineries leads
928 to coccus-to-rod transition and filamentation in ovococci. Mol Microbiol *79*, 759-
929 771.

930 6. Khandige, S., Asferg, C.A., Rasmussen, K.J., Larsen, M.J., Overgaard, M.,
931 Andersen, T.E., and Moller-Jensen, J. (2016). DamX Controls Reversible Cell
932 Morphology Switching in Uropathogenic Escherichia coli. MBio *7*.

933 7. Flardh, K., Richards, D.M., Hempel, A.M., Howard, M., and Buttner, M.J. (2012).
934 Regulation of apical growth and hyphal branching in *Streptomyces*. Curr Opin
935 Microbiol *15*, 737-743.

936 8. Wagner, J.K., Setayeshgar, S., Sharon, L.A., Reilly, J.P., and Brun, Y.V. (2006).
937 A nutrient uptake role for bacterial cell envelope extensions. Proc Natl Acad Sci
938 U S A *103*, 11772-11777.

939 9. Wagner, J.K., and Brun, Y.V. (2007). Out on a limb: how the *Caulobacter* stalk
940 can boost the study of bacterial cell shape. Mol Microbiol *64*, 28-33.

941 10. Abraham, W.-R., Rohde, M., and Bennasar, A. (2014). The Family
942 Caulobacteraceae. In The Prokaryotes: Alphaproteobacteria and
943 Betaproteobacteria, E. Rosenberg, E.F. DeLong, S. Lory, E. Stackebrandt and F.
944 Thompson, eds. (Berlin, Heidelberg: Springer Berlin Heidelberg), pp. 179-205.

945 11. Jiang, C., Brown, P.J., Ducret, A., and Brun, Y.V. (2014). Sequential evolution of
946 bacterial morphology by co-option of a developmental regulator. Nature *506*,
947 489-493.

948 12. Kuhn, J., Briegel, A., Morschel, E., Kahnt, J., Leser, K., Wick, S., Jensen, G.J.,
949 and Thanbichler, M. (2010). Bactofilins, a ubiquitous class of cytoskeletal
950 proteins mediating polar localization of a cell wall synthase in *Caulobacter*
951 *crescentus*. EMBO J *29*, 327-339.

952 13. Sycuro, L.K., Pincus, Z., Gutierrez, K.D., Biboy, J., Stern, C.A., Vollmer, W., and
953 Salama, N.R. (2010). Peptidoglycan crosslinking relaxation promotes
954 *Helicobacter pylori*'s helical shape and stomach colonization. Cell *141*, 822-833.

955 14. Jackson, K.M., Schwartz, C., Wachter, J., Rosa, P.A., and Stewart, P.E. (2018).
956 A widely conserved bacterial cytoskeletal component influences unique helical
957 shape and motility of the spirochete *Leptospira biflexa*. Mol Microbiol *108*, 77-89.

958 15. Randich, A.M., Kysela, D.T., Morlot, C., and Brun, Y.V. (2019). Origin of a Core
959 Bacterial Gene via Co-option and Detoxification of a Phage Lysin. Curr Biol *29*,
960 1634-1646 e1636.

961 16. Billini, M., Biboy, J., Kuhn, J., Vollmer, W., and Thanbichler, M. (2019). A
962 specialized MreB-dependent cell wall biosynthetic complex mediates the
963 formation of stalk-specific peptidoglycan in *Caulobacter crescentus*. PLoS
964 genetics *15*, e1007897.

965 17. Brun, Y.V., and Shapiro, L. (1992). A temporally controlled sigma-factor is
966 required for polar morphogenesis and normal cell division in *Caulobacter*. Genes
967 Dev *6*, 2395-2408.

968 18. Biondi, E.G., Skerker, J.M., Arif, M., Prasol, M.S., Perchuk, B.S., and Laub, M.T.
969 (2006). A phosphorelay system controls stalk biogenesis during cell cycle
970 progression in *Caulobacter crescentus*. Mol Microbiol *59*, 386-401.

971 19. Schmidt, J.M., and Stanier, R.Y. (1966). The development of cellular stalks in
972 bacteria. J Cell Biol *28*, 423-436.

973 20. Gonin, M., Quardokus, E.M., O'Donnol, D., Maddock, J., and Brun, Y.V. (2000).
974 Regulation of stalk elongation by phosphate in *Caulobacter crescentus*. Journal
975 of bacteriology *182*, 337-347.

976 21. Curtis, P.D. (2017). Stalk formation of *Brevundimonas* and how it compares to
977 *Caulobacter crescentus*. PloS one *12*, e0184063.

978 22. Lawler, M.L., and Brun, Y.V. (2007). Advantages and mechanisms of polarity and
979 cell shape determination in *Caulobacter crescentus*. Curr Opin Microbiol *10*, 630-
980 637.

981 23. Thanbichler, M. (2009). Spatial regulation in *Caulobacter crescentus*. Curr Opin
982 Microbiol *12*, 715-721.

983 24. Brown, P.J., Hardy, G.G., Trimble, M.J., and Brun, Y.V. (2009). Complex
984 regulatory pathways coordinate cell-cycle progression and development in
985 *Caulobacter crescentus*. Adv Microb Physiol *54*, 1-101.

986 25. Sundararajan, K., and Goley, E.D. (2017). Cytoskeletal Proteins in *Caulobacter*
987 *crescentus*: Spatial Orchestrators of Cell Cycle Progression, Development, and
988 Cell Shape. Subcell Biochem *84*, 103-137.

989 26. Hughes, H.V., Huitema, E., Pritchard, S., Keiler, K.C., Brun, Y.V., and Viollier,
990 P.H. (2010). Protein localization and dynamics within a bacterial organelle. Proc
991 Natl Acad Sci U S A *107*, 5599-5604.

992 27. Hughes, H.V., Lisher, J.P., Hardy, G.G., Kysela, D.T., Arnold, R.J., Giedroc,
993 D.P., and Brun, Y.V. (2013). Co-ordinate synthesis and protein localization in a
994 bacterial organelle by the action of a penicillin-binding-protein. Mol Microbiol *90*,
995 1162-1177.

996 28. Vasa, S., Lin, L., Shi, C., Habenstein, B., Riedel, D., Kuhn, J., Thanbichler, M.,
997 and Lange, A. (2015). beta-Helical architecture of cytoskeletal bactofilin filaments
998 revealed by solid-state NMR. Proc Natl Acad Sci U S A *112*, E127-136.

999 29. Karimova, G., Pidoux, J., Ullmann, A., and Ladant, D. (1998). A bacterial two-
1000 hybrid system based on a reconstituted signal transduction pathway. Proc Natl
1001 Acad Sci U S A *95*, 5752-5756.

1002 30. Perez, A.M., Mann, T.H., Lasker, K., Ahrens, D.G., Eckart, M.R., and Shapiro, L.
1003 (2017). A Localized Complex of Two Protein Oligomers Controls the Orientation
1004 of Cell Polarity. mBio *8*.

1005 31. Deng, X., Gonzalez Llamazares, A., Wagstaff, J.M., Hale, V.L., Cannone, G.,
1006 McLaughlin, S.H., Kureisaite-Ciziene, D., and Lowe, J. (2019). The structure of
1007 bactofilin filaments reveals their mode of membrane binding and lack of polarity.
1008 Nat Microbiol.

1009 32. den Blaauwen, T., de Pedro, M.A., Nguyen-Disteche, M., and Ayala, J.A. (2008).
1010 Morphogenesis of rod-shaped sacculi. FEMS Microbiol Rev *32*, 321-344.

1011 33. Kuru, E., Hughes, H.V., Brown, P.J., Hall, E., Tekkam, S., Cava, F., de Pedro,
1012 M.A., Brun, Y.V., and VanNieuwenhze, M.S. (2012). *In Situ* probing of newly
1013 synthesized peptidoglycan in live bacteria with fluorescent D-amino acids. Angew
1014 Chem Int Ed Engl *51*, 12519-12523.

1015 34. Brown, P.J., Kysela, D.T., and Brun, Y.V. (2011). Polarity and the diversity of
1016 growth mechanisms in bacteria. Semin Cell Dev Biol *22*, 790-798.

1017 35. Pinho, M.G., Kjos, M., and Veening, J.W. (2013). How to get (a)round:
1018 mechanisms controlling growth and division of coccoid bacteria. Nature reviews.
1019 Microbiology *11*, 601-614.

1020 36. Radhakrishnan, S.K., Thanbichler, M., and Viollier, P.H. (2008). The dynamic
1021 interplay between a cell fate determinant and a lysozyme homolog drives the
1022 asymmetric division cycle of *Caulobacter crescentus*. Genes Dev *22*, 212-225.

1023 37. Wali, T.M., Hudson, G.R., Danald, D.A., and Weiner, R.M. (1980). Timing of
1024 swarmer cell cycle morphogenesis and macromolecular synthesis by
1025 *Hyphomicrobium neptunium* in synchronous culture. Journal of bacteriology *144*,
1026 406-412.

1027 38. Moore, R.L. (1981). The biology of *Hyphomicrobium* and other prosthecate,
1028 budding bacteria. Annu Rev Microbiol *35*, 567-594.

1029 39. Zerfas, P.M., Kessel, M., Quintero, E.J., and Weiner, R.M. (1997). Fine-structure
1030 evidence for cell membrane partitioning of the nucleoid and cytoplasm during bud
1031 formation in *Hyphomonas* species. Journal of bacteriology *179*, 148-156.

1032 40. Cserti, E., Rosskopf, S., Chang, Y.W., Eisheuer, S., Selter, L., Shi, J., Regh, C.,
1033 Koert, U., Jensen, G.J., and Thanbichler, M. (2017). Dynamics of the
1034 peptidoglycan biosynthetic machinery in the stalked budding bacterium
1035 *Hyphomonas neptunium*. Mol Microbiol *103*, 875-895.

1036 41. Meniche, X., Otten, R., Siegrist, M.S., Baer, C.E., Murphy, K.C., Bertozzi, C.R.,
1037 and Sassetti, C.M. (2014). Subpolar addition of new cell wall is directed by
1038 DivIVA in mycobacteria. Proc Natl Acad Sci U S A *111*, E3243-3251.

1039 42. Melzer, E.S., Sein, C.E., Chambers, J.J., and Sloan Siegrist, M. (2018). DivIVA
1040 concentrates mycobacterial cell envelope assembly for initiation and stabilization
1041 of polar growth. Cytoskeleton (Hoboken) *75*, 498-507.

1042 43. Kysela, D.T., Randich, A.M., Caccamo, P.D., and Brun, Y.V. (2016). Diversity
1043 Takes Shape: Understanding the Mechanistic and Adaptive Basis of Bacterial
1044 Morphology. PLoS Biol *14*, e1002565.

1045 44. Taylor, J.A., Sichel, S.R., and Salama, N.R. (2019). Bent Bacteria: A Comparison
1046 of Cell Shape Mechanisms in Proteobacteria. Annu Rev Microbiol *73*, 457-480.

1047 45. Poindexter, J.S. (1978). Selection for nonbuoyant morphological mutants of
1048 *Caulobacter crescentus*. Journal of bacteriology *135*, 1141-1145.

1049 46. Dower, W.J., Miller, J.F., and Ragsdale, C.W. (1988). High efficiency
1050 transformation of *E. coli* by high voltage electroporation. Nucleic acids research
1051 *16*, 6127-6145.

1052 47. Chung, C.T., Niemela, S.L., and Miller, R.H. (1989). One-step preparation of
1053 competent *Escherichia coli*: transformation and storage of bacterial cells in the
1054 same solution. Proc Natl Acad Sci U S A *86*, 2172-2175.

1055 48. Chung, C.T., and Miller, R.H. (1993). Preparation and storage of competent
1056 *Escherichia coli* cells. Methods Enzymol *218*, 621-627.

1057 49. Saltikov, C.W., and Newman, D.K. (2003). Genetic identification of a respiratory
1058 arsenate reductase. Proc Natl Acad Sci U S A *100*, 10983-10988.

1059 50. Thanbichler, M., Iniesta, A.A., and Shapiro, L. (2007). A comprehensive set of
1060 plasmids for vanillate- and xylose-inducible gene expression in *Caulobacter*
1061 *crescentus*. Nucleic acids research *35*, e137.

1062 51. Chen, I.A., Chu, K., Palaniappan, K., Pillay, M., Ratner, A., Huang, J.,
1063 Huntemann, M., Varghese, N., White, J.R., Seshadri, R., et al. (2019). IMG/M
1064 v.5.0: an integrated data management and comparative analysis system for
1065 microbial genomes and microbiomes. Nucleic acids research *47*, D666-D677.

1066 52. Waterhouse, A.M., Procter, J.B., Martin, D.M., Clamp, M., and Barton, G.J.
1067 (2009). Jalview Version 2--a multiple sequence alignment editor and analysis
1068 workbench. Bioinformatics *25*, 1189-1191.

1069 53. Waterhouse, A., Bertoni, M., Bienert, S., Studer, G., Tauriello, G., Gumienny, R.,
1070 Heer, F.T., de Beer, T.A.P., Rempfer, C., Bordoli, L., et al. (2018). SWISS-
1071 MODEL: homology modelling of protein structures and complexes. Nucleic acids
1072 research *46*, W296-W303.

1073 54. Robert, X., and Gouet, P. (2014). Deciphering key features in protein structures
1074 with the new ENDscript server. Nucleic acids research *42*, W320-324.

1075 55. Raghava, G.P., and Barton, G.J. (2006). Quantification of the variation in
1076 percentage identity for protein sequence alignments. BMC Bioinformatics *7*, 415.

1077 56. Schindelin, J., Arganda-Carreras, I., Frise, E., Kaynig, V., Longair, M., Pietzsch,
1078 T., Preibisch, S., Rueden, C., Saalfeld, S., Schmid, B., et al. (2012). Fiji: an open-
1079 source platform for biological-image analysis. Nat Methods *9*, 676-682.

1080 57. Ducret, A., Quardokus, E.M., and Brun, Y.V. (2016). MicrobeJ, a tool for high
1081 throughput bacterial cell detection and quantitative analysis. Nat Microbiol *1*,
1082 16077.

1083 58. Tinevez, J.Y., Perry, N., Schindelin, J., Hoopes, G.M., Reynolds, G.D.,
1084 Laplantine, E., Bednarek, S.Y., Shorte, S.L., and Eliceiri, K.W. (2017).
1085 TrackMate: An open and extensible platform for single-particle tracking. Methods
1086 *115*, 80-90.

1087 59. R Development Core Team (2012). R: a language and environment for statistical
1088 computing. (Vienna, Austria: The R Foundation for Statistical Computing).

1089 60. Wickham, H. (2016). ggplot2: Elegant Graphics for Data Analysis. (New York:
1090 Springer-Verlag).

1091 61. Ahlmann-Eltze, C. (2019). ggsignif: Significance Brackets for 'ggplot2'. 0.5.0
1092 Edition.

1093 62. Pate, J.L., and Ordal, E.J. (1965). The fine structure of two unusual stalked
1094 bacteria. J Cell Biol *27*, 133-150.

1095 63. Shi, C., Fricke, P., Lin, L., Chevelkov, V., Wegstroth, M., Giller, K., Becker, S.,
1096 Thanbichler, M., and Lange, A. (2015). Atomic-resolution structure of cytoskeletal
1097 bactofilin by solid-state NMR. Sci Adv *1*, e1501087.

1098 64. Mcgill, R., Tukey, J.W., and Larsen, W.A. (1978). Variations of Box Plots. Am
1099 Stat *32*, 12-16.

1100 65. Hintze, J.L., and Nelson, R.D. (1998). Violin Plots: A Box Plot-Density Trace
1101 Synergism. The American Statistician *52*, 181-184.

1102